Title:

An experimental study of a rectangular floating breakwater with flexible curtains as

wave-dissipating components

Author names and affiliations:

Fang He[1, 2], Jiapeng Pan[2], Jindi Li[2], Siming Zheng[2]*, Zhiming Yuan[3]

[1]Donghai Laboratory, Zhoushan, Zhejiang 316021, China

[2]Ocean College, Zhejiang University, Zhoushan, Zhejiang 316021, China

[3]Department of Naval Architecture, Ocean and Marine Engineering, University of

Strathclyde, Glasgow, G4 0LZ, UK

***Corresponding author**. E-mail address: siming.zheng@zju.edu.cn

An experimental study of a rectangular floating breakwater with flexible curtains as wave-dissipating components

Abstract

In this study, the flexible curtains are attached to the bottom of a rectangular floating breakwater as wave-dissipating components. Through a comprehensive experimental investigation, the wave attenuation, motion responses, and mooring forces of the proposed floating breakwater are examined, with a particular focus on the effects of wave height and the hanging length and porosity of the flexible curtain. Meanwhile, comparative analyses are conducted with the stand-alone rectangular floating breakwater and with attaching one rigid slotted barrier. Our experimental results indicate that one underhanging flexible curtain can augment wave attenuation across all tested wave conditions, which is comparable to the rigid slotted barrier. Furthermore, attaching two flexible curtains contributes to a more significant enhancement for harbor or coastal protection, especially against long waves. This can be attributed to the buffer function of flexible curtains, and the increased added mass induced by the water body confined between them, which increases the natural period of floating breakwaters. Furthermore, the attachment of the flexible curtains significantly suppresses the motion responses of the breakwater, which can alleviate the undesirable strong mooring forces. In general, increasing the length or decreasing the porosity of flexible curtains leads to similar trends in the performance of floating breakwaters. The flexible curtains have been proven to be effective wave-dissipating components for rectangular floating breakwaters.

Keywords: Floating breakwater; Flexible curtain; Wave attenuation; Wave transmission; Motion response; Mooring force

1. Introduction

Floating breakwaters are generally employed to protect coastlines, small marinas, recreational harbors, and fish cages against wave attacks, and may be preferred in locations with relatively large water depths, high tidal variation, and poor foundation (Dong et al., 2008; Li et al., 2022). They could also provide temporary protection against waves for offshore activities such as marine construction and maintenance. Compared to bottom-mounted breakwaters, floating breakwaters have the advantages of being environmentally friendly, rapidly deployable, multifunctional, and aesthetic, which advocate their application in certain ocean engineering with corresponding considerations (Dai et al., 2018; He et al., 2013). However, the wave attenuation of floating breakwater is still unsatisfactory and requires enhancement, especially for medium and long waves.

Given the property of wave energy to concentrate near the surface of the water (Drew et al., 2009), the floating breakwater has the potential to effectively attenuate wave energy. For the floating breakwater, its transmitted waves are the superposition of scattered waves beneath it and motion-induced radiated waves (Adee, 1976; He et al., 2023). Therefore, the wave attenuation of the floating breakwater can be achieved by wave reflection, wave energy dissipation, and the reduction of radiated waves (Hales, 1981; Yang et al., 2021). For effective reflection, it is essential to ensure a substantial draft and minimize the amplitude of motion of the floating breakwaters. In this way, the radiated waves are also suppressed. As for enhancing wave energy dissipation, strategies such as amplifying the friction between the water body and the structure, triggering wave-breaking, inducing vortex shedding, and encouraging water-body resonance can be employed (Cheng et al., 2022; Dai et al., 2018; Ji et al., 2023).

Various novel types of floating breakwaters have been proposed. Hales (1981), McCartney (1985), and Dai et al. (2018) conducted comprehensive surveys of floating breakwaters sequentially, and floating breakwaters are subdivided into several categories based on their configurations or wave attenuation mechanism. Among the plethora of floating breakwater designs, the rectangular box-type floating breakwater is the most widespread due to its simplistic geometry, durability, and multifunctional potential, such as boat moorings and walkways (Jin et al., 2022; Mohapatra et al., 2024). Consequently, many scholars investigated its hydrodynamic characteristics and motion response theoretically (Alamailes and Türker, 2019), numerically (Chen et al., 2022), and experimentally (Liang et al., 2022). However, there is a consensus that while the rectangular floating breakwater effectively attenuates short-period waves, it falls short

of effectively attenuating long-period waves (Ji et al., 2018).

To enhance the wave attenuation of floating breakwaters, one could consider adopting vertical piles (Ning et al., 2016; Yin et al., 2023) or taut mooring systems (Rahman et al., 2006; Zhang et al., 2023) to restrain the motions of the floating breakwater, leading to a reduction in motion-induced radiated waves. Nevertheless, large water depths and poor foundations will preclude their utility. In addition, the wear problem between piles and the moving breakwater is inevitable (Falcão and Henriques, 2014; McCartney, 1985). In the context of taut mooring, the mooring chain needs to suffer large impulsive forces due to the wave attack (Qiao et al., 2020). Excessive mooring forces may give rise to the failure of the mooring line systems or the offset of anchors (Wang et al., 2021). Hence, while vertical piles and taut mooring systems can enhance the wave attenuation of floating breakwaters, they concurrently elevate requirements in the application. In contrast, though the slack mooring systems do not impede motion as expected, they are a more plausible choice in deep waters and areas with weak foundations, and have the advantage of rapid deployment, making full use of the advantages of floating breakwaters.

Another viable strategy is to optimize the superstructure, i.e., the floating box, to promote wave attenuation. Attaching wave-dissipating components to floating box is an efficient and cost-effective approach, such as wing plates (Han and Dong, 2023; Liu et al., 2019), porous structures (Ji et al., 2019; Zheng et al., 2018), underhanging barriers (Deng et al., 2019; Rageh and Koraim, 2010) and pneumatic chambers (He et al., 2017; Howe et al., 2020). Among these, underhanging barriers are often favored given that they excel in enhancing wave reflection as well. Comparatively, rigid slotted barriers, which comprise an array of closely spaced cylinders, are preferable for augmenting wave energy dissipation, as opposed to attaching rigid solid barriers (Murali et al., 2005; Murali and Mani, 1997). Meanwhile, the slotted structure can mitigate the effects of wave loading as well (Chanda and Bora, 2020; Chanda and Pramanik, 2023). Huang et al. (2014) experimentally investigated the hydrodynamic performance of the rectangular floating breakwater with rigid slotted barriers. They found that attaching rigid slotted barriers resulted in a smaller transmission coefficient, especially for long waves. More recently, He et al. (2023) studied the effect of mounting position, mounting rows, porosity, and barrier height further on the performance of a rectangular floating breakwater and discovered that the water body confined by barriers plays a significant role in the dynamic characteristics of floating breakwaters.

However, though rigid barriers are slotted, they still tend to increase the mooring

forces of the box-type floating breakwaters (He et al., 2023; Nasri et al., 2021), which is detrimental to their reliability and survivability. Kim and Kee (1996) pointed out that a more flexible structure led to smaller forces acting on the membrane and mooring lines. In addition, Li et al. (2022) and Sun et al. (2022) integrated kelp into the twin pontoon and box-type floating breakwater, respectively, and found the kelp array is helpful to long-wave attenuation. Given these, we attached the flexible curtain as wave-dissipating components to the bottom of the floating breakwater and examined its performance. The flexible curtain could extend to the seabed with an expectation of not causing much force to the mooring lines. A slack mooring line system was adopted to resist the mean drift force and hold the floating breakwater at the dynamic equilibrium position. Each flexible curtain consists of a row of nylon ropes with the same diameter. The diameter can be desirably selected to ensure that the nylon ropes possess sufficient stiffness to resist drifting caused by waves. The bottom of the rope is fixed to a thin and long acrylic block, which is lightweight and is only used to keep all ropes moving in unison. This differs from the flexible membrane (Cho et al., 1997; Guo et al., 2023) and net (Cheng et al., 2021; Ji et al., 2017) in the literature, whose tension was achieved by hinging to the seafloor and hanging clump weight, respectively.

In the present study, the wave attenuation, motion responses, and mooring forces of floating breakwaters are investigated based on physical model experiments, specifically examining the effects of wave height, the hanging length, and the porosity of the flexible curtain on them. Furthermore, both the stand-alone rectangular floating breakwater and the one equipped with an attached rigid slotted barrier are examined for comparison to assess the effectiveness of the proposed floating breakwater. This study seeks to illustrate that long flexible curtains effectively mitigate the motion responses of floating breakwaters without inducing significant mooring forces. Serving as wave-dissipating components, these flexible curtains offer an economical and feasible means to enhance the performance of rectangular floating breakwaters in longer waves. The subsequent sections are organized as follows: Section 2 provides a detailed description of the physical models, experimental setup, and data acquisition methods. Section 3 examines the impact of wave height, hanging length, and porosity on wave attenuation, motion response, and mooring force, and includes a comparative analysis of transmission coefficients across different types of floating breakwaters. Section 4 presents the main conclusions.

2. Experimental procedure

2.1. Physical models

The experiments are scaled according to the Froude criterion. In accordance with the experimental instruments, facilities of the laboratory, and the tested conditions, the geometric scale of 1:25 is selected in this study. The physical models involved in this study are composed of a rectangular floating box and one or two underhanging components. The rectangular floating box (see Fig. 1) is made of Perspex sheets. The external frame of the box is constructed using 10 mm thick Perspex sheets, while 5 mm thick Perspex sheets are utilized to partition the internal tank for the steel ballasts. The overall rectangular floating box is 680 mm long, 500 mm wide, and 250 mm high. Two omnidirectional ball bearings are affixed to each lateral side of the model to prevent any potential collisions with the walls of the flume. The underhanging component (see Fig. 2) comprises either the rigid slotted barrier or the flexible curtain (see Fig. 3) and is mounted on the bottom of the box with the slotted feature. The vertical units comprising the rigid slotted barrier and the flexible curtain are constructed by a PVC circular cylinder and a nylon rope, respectively, each with a 20 mm diameter. The gap between two adjacent units is denoted as e_1, and the distance between the outermost unit and the side of the box is e_2. The porosity p is determined by the number of units, and the arrangement of them is associated with e_1 and e_2, which are illustrated in Table 1. For securing vertical units and easy installation, the top and bottom sides of the vertical units are fitted with two acrylic panels, and the density, thickness, and width of each panel are 1.2 g/cm^3, 10 mm, and 25mm, respectively. As shown in Fig. 2, the vertical unit's length l_s has three values (73, 143, and 213 mm). Consequently, the hanging length of the underhanging barrier l can be either 93, 163, or 233 mm. A centrosymmetric arrangement is always maintained no matter one or two underhanging components (see Fig. 4), and the distance between two underhanging components is 375 mm when two barriers are attached. The draft of the rectangular floating box Dr is fixed at 130 mm for every tested model by adjusting ballasts, which makes the gravity center below the buoyant center and the freeboard high enough to avoid overtopping. In summary, this research tested 19 different floating breakwater models, which can be classed into four types: Type I: rectangular floating box; Type II: rectangular floating box with one rigid slotted barrier; Type III: rectangular floating box with one flexible curtain; Type IV: rectangular floating box with two flexible curtains. More details can be found in Table 2.
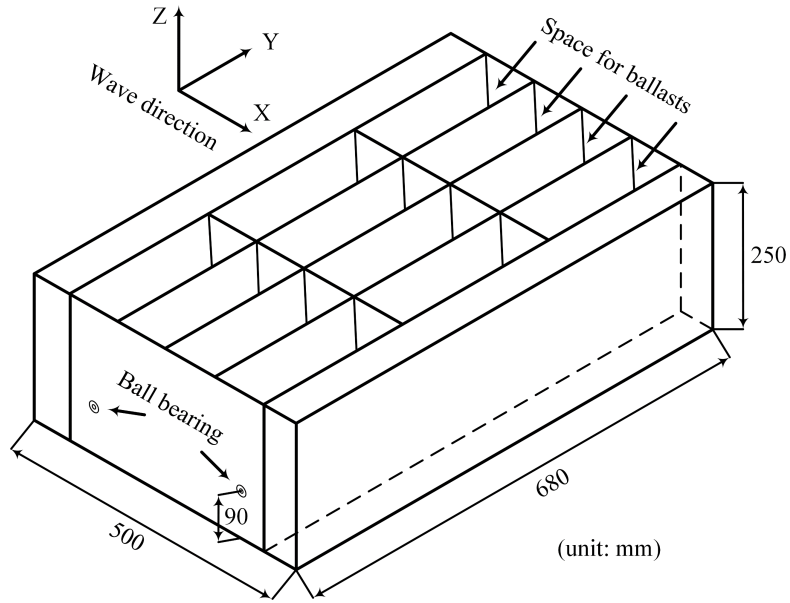
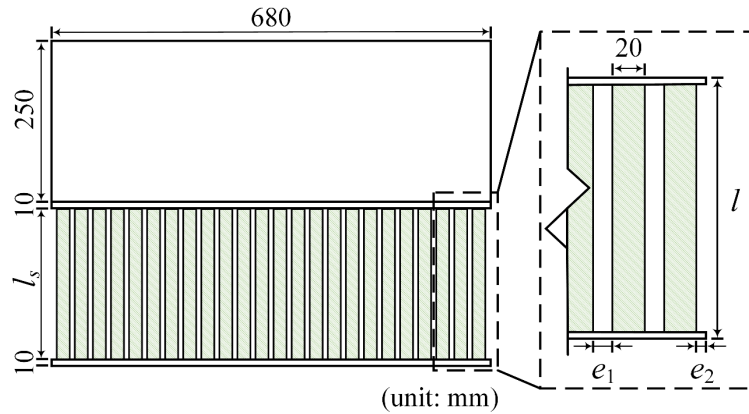Fig. 1 Details of the rectangular floating box model.

Fig. 2 Sketch of the rectangular floating breakwater with underhanging component
(front view)

Fig. 3 A view of two types of underhanging component

Table1 Details of the underhanging component

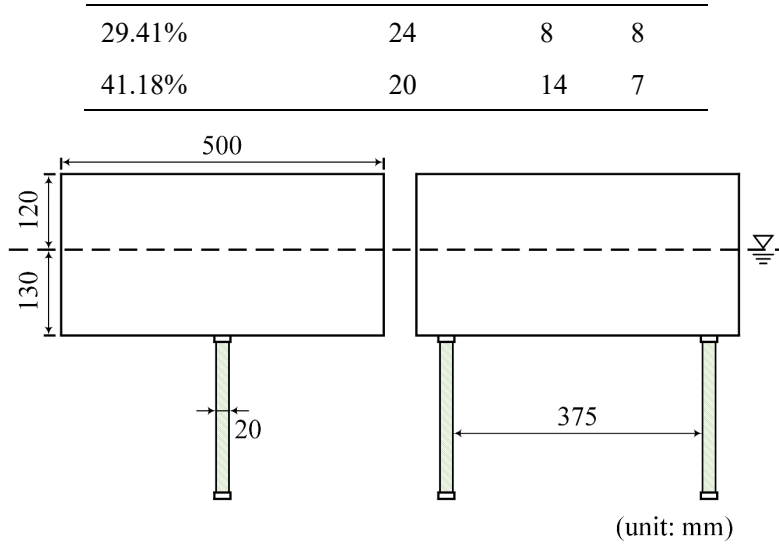| Porosity of the barriers	Number of units	e_1 (mm)	e_2 (mm)
5.88%	32	1	4.5
17.65%	28	4	6

29.41%	24	8	8
41.18%	20	14	7

(unit: mm)

Fig. 4 Sketch of rectangular floating breakwater with one or two underhanging components (side view)

Table 2 Details of the tested models in the experiments.

Type	Model	Type of components	Number of components	l (mm)	Porosity p	Mass (kg)	GC above the bottom (mm)	Moment of inertia (kg·m^2)
Type I	Model 1	/	/	/	/	43.87	51.09	1.032
Type II	Model 2	Rigid	One	93	5.88%	44.61	49.53	1.042
Type II	Model 3	Rigid	One	163	5.88%	45.36	47.6	1.064
Type II	Model 4	Rigid	One	233	5.88%	46.11	45.08	1.087
Type II	Model 5	Rigid	One	233	17.65%	45.94	45.69	1.082
Type II	Model 6	Rigid	One	233	29.41%	45.77	46.30	1.076
Type II	Model 7	Rigid	One	233	41.18%	45.27	47.07	1.076
Type III	Model 8	Flexible	One	93	5.88%	44.57	49.60	1.042
Type III	Model 9	Flexible	One	163	5.88%	44.95	47.97	1.056
Type III	Model 10	Flexible	One	233	5.88%	45.33	45.77	1.081
Type III	Model 11	Flexible	One	233	17.65%	45.18	46.34	1.076
Type III	Model 12	Flexible	One	233	29.41%	45.02	46.91	1.072
Type III	Model 13	Flexible	One	233	41.18%	44.86	47.49	1.067
Type IV	Model 14	Flexible	Two	93	5.88%	45.26	48.16	1.172
Type IV	Model 15	Flexible	Two	163	5.88%	46.02	44.99	1.281
Type IV	Model 16	Flexible	Two	233	5.88%	47.11	40.69	1.440
Type IV	Model 17	Flexible	Two	233	17.65%	46.8	41.75	1.420
Type IV	Model 18	Flexible	Two	233	29.41%	46.49	42.83	1.399
Type IV	Model 19	Flexible	Two	233	41.18%	45.85	44.04	1.372

2.2. Experimental setup and wave conditions

The physical model tests are conducted in a glass-walled wave flume located at the Port & Offshore Engineering Laboratory of Zhejiang University, China. The wave flume is 25 m long, 0.7 m wide, and 0.7 m high, as shown in the left panel of Fig. 5. A piston-type wave maker with an active absorption control system is installed at one end of the wave flume, and the other end equips the 1:6 wave absorbing beach made of porous media to absorb the transmitted wave. Based on the pre-test examination, the wave reflection of the empty flume is less than 5% for the tested wave conditions.

Fig. 6 illustrates the experimental arrangement. The floating breakwater is slack-moored at a distance of 13 meters from the wave maker, positioned at its dynamic equilibrium. Two sets of mooring chains are affixed to the front and rear sides of the floating breakwater, with each set linked to a steel anchor. The stainless-steel mooring chains, each measuring 3 m in length with a line density of 0.1475 kg/m, are accompanied by steel anchors characterized by small dimensions (0.1m×0.1m×0.04m) that minimally impact the wave field. Each anchor weighs 3.2 kg and is kept 2.9 m away from the nearest side of the floating breakwater. The length of the mooring chain is long enough to maintain the slack condition of mooring chains, meanwhile, the weight of the steel anchor is proven to prevent offsetting in the experimental process. The motions of the floating breakwater are constrained to two-dimensional by the two ball bearings installed on each lateral side (see the right panel of Fig. 5).

The parametric study is performed under normal regular waves with periods ranging from 0.8s to 1.7s at a 0.1s interval, and the water depth for all experimental conditions is fixed at 0.4 m. Details of test conditions are summarized in Table 3.

Fig. 5 Views of both the glass-walled wave flume (left panel) and the physical model in the wave flume (right panel).
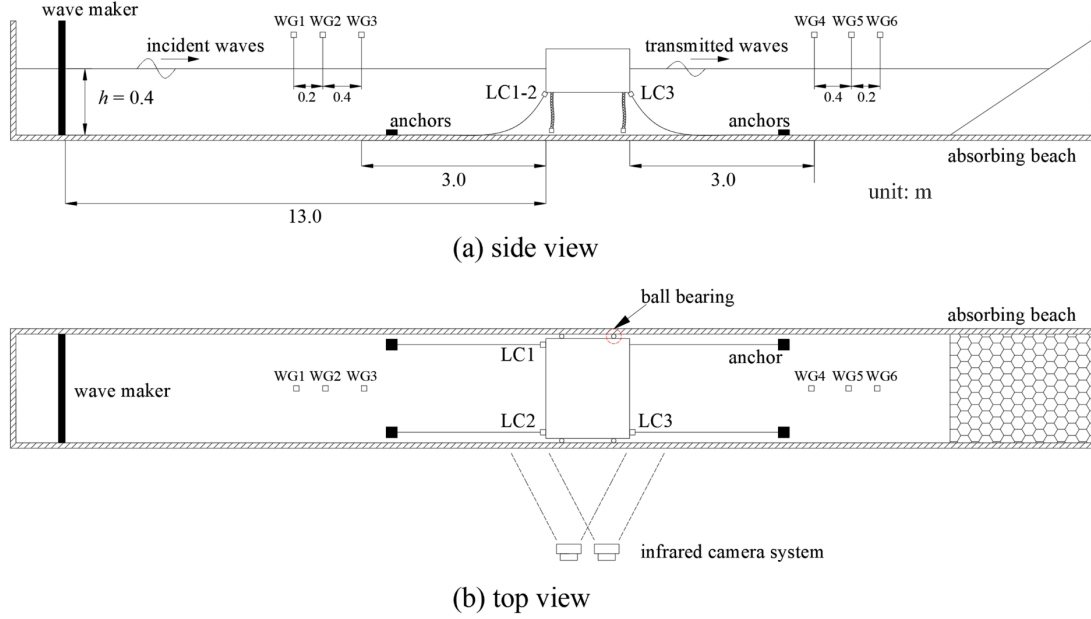
(a) side view

(b) top view

Fig. 6 Sketch of the experimental setup (unit: m)

Table 3 Experimental test conditions.

Parameters	Ranges
Water depth, h	0.40 m
Wave height, H_i	0.02, 0.03, 0.04 m
Wave period, T	0.8-1.7 s at 0.1 s interval
Wave length, L	0.986-3.052 m

2.3. Data acquisition and processing

Six HR Wallingford wave gauges (WG1-6) are arranged to monitor the surface elevation. WG1-3 are placed in the seaside of the model, while WG4-6 are placed in the leeside of the model. The distances between wave gauges are shown in Fig. 6. The wave gauge is calibrated before and after each test to guarantee the accuracy of wave measurement. The two-point method presented by Goda and Suzuki (1976) is used to resolve the incident and reflected waves from the simultaneous wave records of WG1-3 and resolve the transmitted wave and the possible reflected wave from the absorbing beach based on the records of WG4-6. Here we denote the amplitudes of incident, reflected, and transmitted waves as A_i, A_r, and A_t, respectively. The reflection coefficient C_r and the transmission coefficient C_t are defined as A_r/A_i and A_t/A_i. The wave power dissipation coefficient C_d is the ratio between the dissipated wave power and incident wave power. C_d can be calculated by the equation of wave energy conservation as follow:

$$C_r^2 + C_t^2 + C_d = 1. \tag{1}$$

The motion responses of the floating breakwater are recorded using the Qualisys motion capture system, comprising two infrared cameras, a Qualisys tracking manager for acquiring and processing motion data, and several retro-reflective markers. We define the surge RAO, heave RAO, and pitch RAO as A_{surge}/A_i, A_{heave}/A_i, and $A_{pitch}W/A_i$ respectively, where A_{surge}, A_{heave}, and A_{pitch} are the oscillating amplitudes of the breakwater in surge, heave, and pitch, respectively, and W the width of the breakwater, which is 0.5 m.

Three resistance-type load cells are installed between the model and mooring lines to measure mooring forces, of which two load cells (LC1 and LC2 in Fig. 6) are connected to the seaward mooring lines and one load cell (LC3 in Fig. 6) is connected to one of the leeward mooring lines. The results of mooring forces are presented by their normalized forms of the seaward ($f_s/\gamma WA_i$) and leeward mooring forces ($f_l/\gamma WA_i$), in which f_s, f_l, and γ are seaward mooring force per unit length of mooring chain, leeward mooring force per unit length of mooring chain and unit weight of seawater, respectively.

In the Appendix, time histories of free surface elevations recorded by the wave gauges, the mooring forces and the breakwater motion responses of one typical test case are shown in Fig. A1.

3. Results and discussion

3.1. Effects of wave height

Within this section, Models 1, 4, 10, and 16 are chosen to illustrate how wave height influences the performance of four distinct types of floating breakwaters, examining aspects such as wave reflection, wave transmission, wave power dissipation, motion responses, and mooring forces, with fixed values of l and p at 233 mm and 5.88%, respectively.

3.1.1. Reflection, transmission, and wave power dissipation coefficients

Fig. 7 presents the variation in C_r as a function of the relative width W/L for four types of floating breakwater under three wave heights. It is observed that H_i minimally influences C_r across four types of breakwater. In the case of Type III, C_r exhibits a monotonic increase, ranging from a minimum value of 0.05 to a maximum value of 0.74, with the increase in W/L. The overall trend indicates an increase in C_r for Types I, II, and IV with a rising W/L. Nevertheless, there is a localized decrease in C_r within a

specific range of wave periods.

Fig. 8 shows the variation in C_t versus W/L for four types under three wave heights. The results show that the increase in H_i incurs a slight decrease in C_t for Types I, II, and III over a wide range of wave periods, whereas the smaller H_i exhibits a larger C_t for Type IV when $0.19 < W/L < 0.29$. The minimum of C_t for Types I, II, and III occurs at $W/L = 0.34$, whilst for Type IV it appears at $W/L = 0.29$. The comparison of C_t for Types I, II, and III indicates that the addition of one rigid slotted barrier or flexible curtain with length and porosity being 233 mm and 5.88% enables significant improvement in the wave attenuation performance of the rectangular box-type floating breakwater for relatively short and medium periods waves. In addition, it is observed that C_t for Type IV is significantly smaller than those of Types I, II, and III when $W/L < 0.3$, demonstrating that attaching two flexible curtains to the rectangular floating breakwater can further improve its effectiveness of attenuating long-wave energy. Generally, $C_t < 0.5$ means the breakwater has effective wave attenuation performance (Koutandos et al., 2005; Ning et al., 2016). Therefore, in terms of the W/L range that achieves effective wave attenuation, Type IV is the best.

The variation in C_d as a function of W/L for four types under three wave heights is illustrated in Fig. 9. The results indicate that a larger H_i is accompanied by a larger C_d for Types I, II, and III over a wide range of wave periods, but results in a smaller C_d for Type IV when $0.19 < W/L < 0.26$. The maximum C_d of Types I, II, III, and IV occurs at $W/L = 0.34$, 0.29, 0.34, and 0.26, respectively. Moreover, Type IV is capable of dissipating much more wave power than Types I, II, and III when $W/L < 0.26$ for any specified H_i. This result, together with Fig.7, shows that under long wave conditions, the lower C_t that Type IV maintains is mainly attributed to its stronger wave dissipation capacity.

Since the insensitivity of C_r to changes in H_i for all tested types of breakwater, it is noteworthy that the C_t and C_d are basically negatively correlated in response to changes in H_i. For the rectangular breakwaters, the vortex shedding around the sharp edge is believed to play an important role in wave power dissipation (He et al., 2023; Rageh and Koraim, 2010; Yang et al., 2018). Through numerical simulation, when increasing H_i, the more violent vortex shedding, which is a viscous, nonlinear process, may lead to an increase in C_d. Hence a lower C_t is generally achieved for a larger H_i. However, for the floating breakwater with two flexible curtains, the effect of increasing H_i is opposite in some specified medium waves ($0.20 < W/L < 0.35$). For those special scenarios, water waves with small H_i are likely to be efficiently trapped between the

two curtains and difficult to transmit to the back of the breakwater. Since the length of the curtains is fixed, the trapping effect becomes weakened with the increase in H_i, resulting in a larger C_t and a lower C_d.
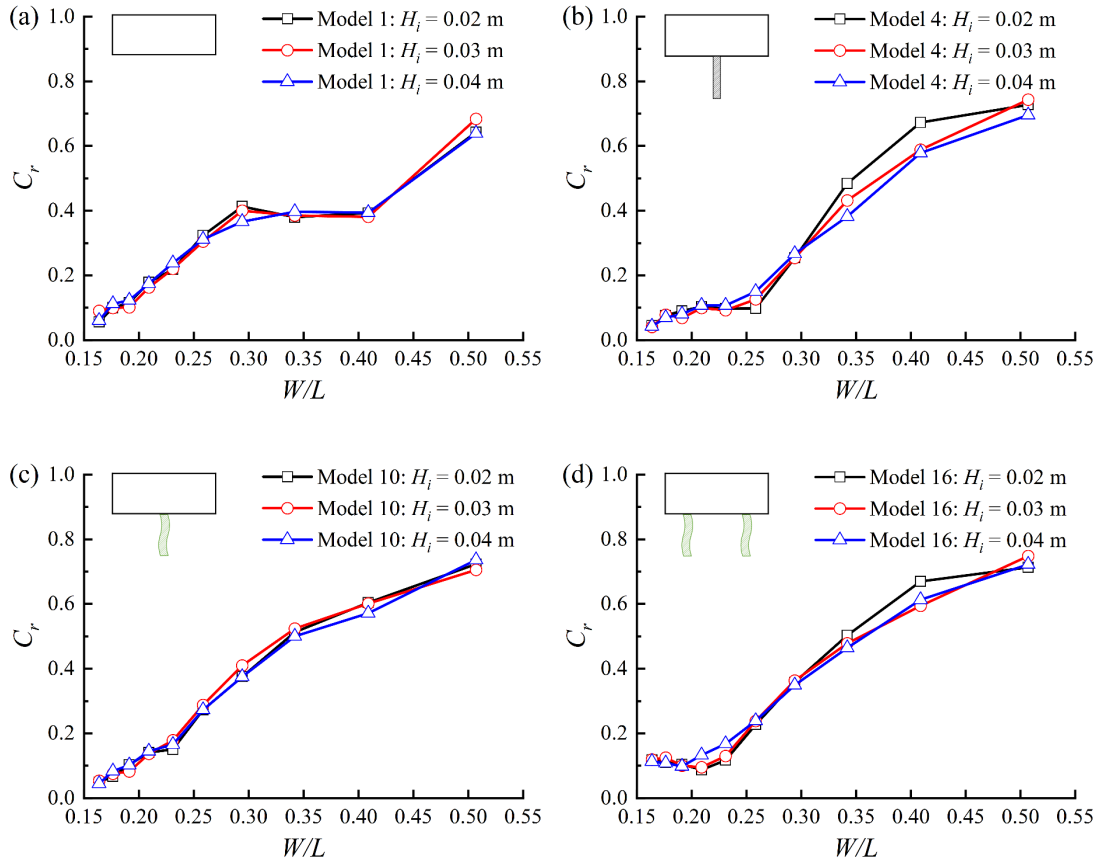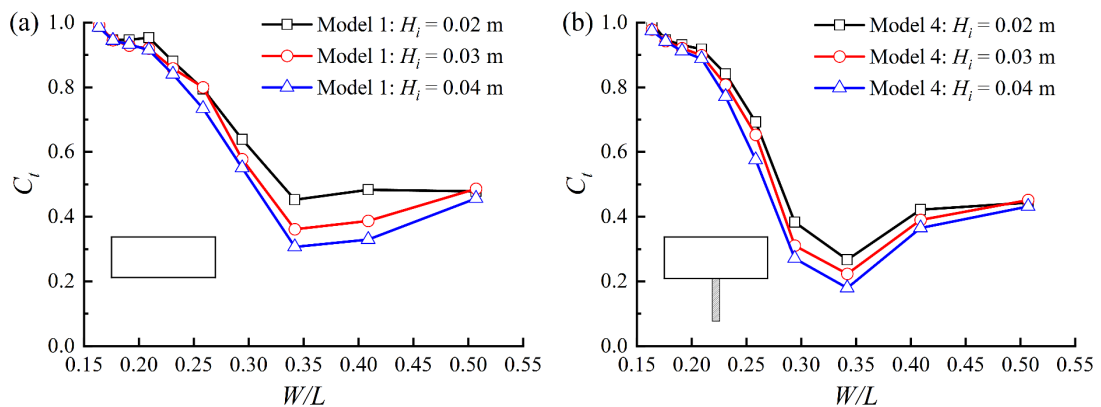

Fig. 7 Variation in reflection coefficient C_r versus W/L under three wave heights: (a) Type I; (b) Type II; (c) Type III; (d) Type IV.
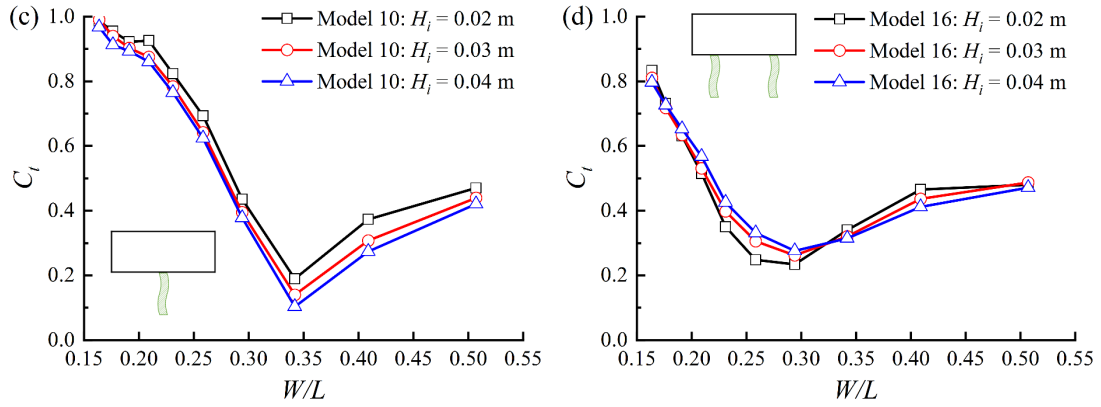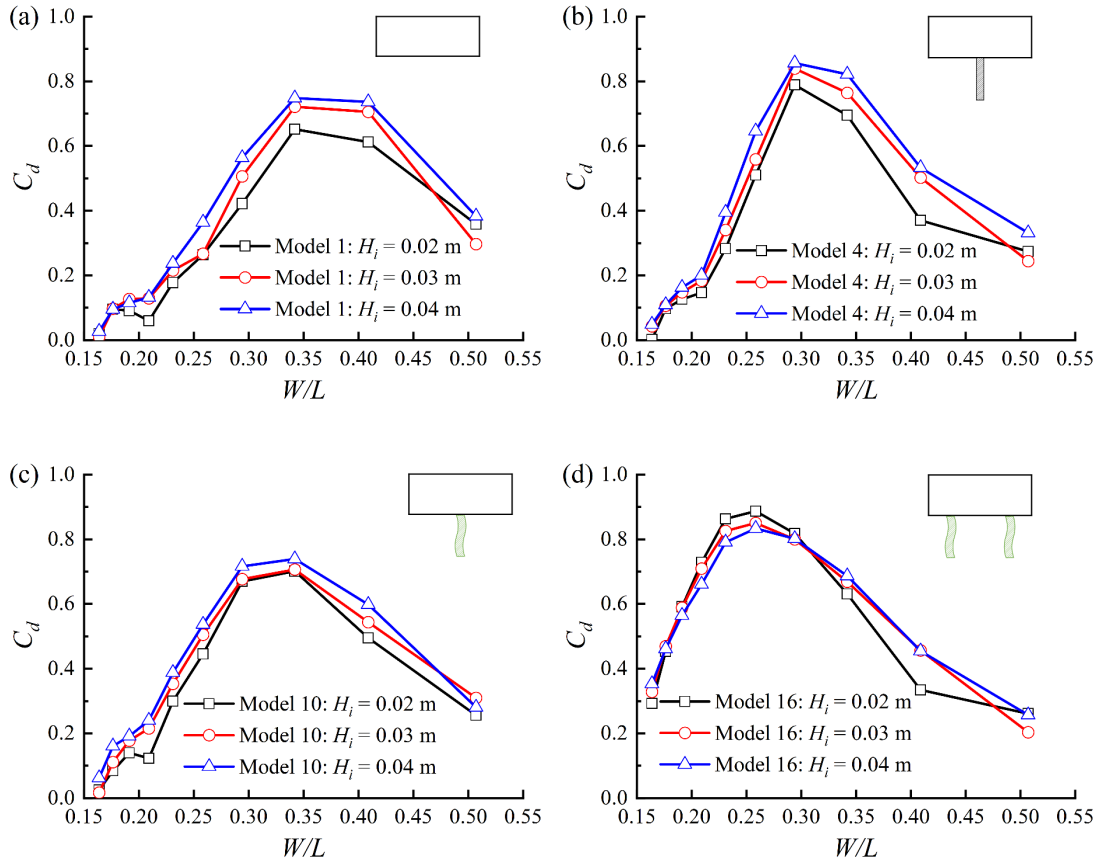
Fig. 8 Variation in transmission coefficient C_t versus W/L under three wave heights: (a) Type I; (b) Type II; (c) Type III; (d) Type IV.

Fig. 9 Variation in wave power dissipation coefficient C_d versus W/L under three wave heights: (a) Type I; (b) Type II; (c) Type III; (d) Type IV.

3.1.2. Surge, heave and pitch RAOs

The variation in surge RAOs of four types of floating breakwater versus W/L under three wave heights are given in Fig. 10. The results show that H_i has little effect on the surge RAOs for four types except Type IV at $W/L < 0.21$, where an undeniable rise in

14

the surge RAO coincides with the increase in the H_i. The surge RAO presents an overall decreasing trend with the increase in W/L for all the examined types of floating breakwater, although a relatively small local valley of the surge RAO-W/L curve may occur, e.g., the Type I case around $W/L = 0.41$. For long-period waves, e.g., $W/L<0.25$, the surge RAOs of Types II and III are smaller than that of Type I, meaning that the surge motion of the rectangular breakwater can be effectively reduced by introducing either a rigid slotted barrier or a flexible curtain. As shown in Fig. 10d, a further decrease in the surge RAO for $W/L<0.25$ can be achieved by adopting two flexible curtains.

Fig. 11 shows the variation in heave RAOs versus W/L for four types of floating breakwaters under three wave heights. The influence of the H_i mainly occurs at $0.16<W/L<0.34$, for which the larger the H_i, the slightly smaller the heave RAO regardless of the types of the floating breakwater. The variation in heave RAOs for Types I, II, and III versus W/L demonstrates a consistent trend: as W/L decreases, they increase gradually first, and subsequently exhibit minimal changes after achieving their peak value. We can call it the peak plateau state when the heave RAO maintains high and constant values in long waves, and there is a W/L value as a threshold for this state. For Types I, II, and III tested in Section 3.1, the threshold is 0.26. In contrast, there is no peak plateau state observed for the heave RAO - W/L curves of Type IV and it consistently diminishes in a monochromatic manner as the W/L increases. It is considerably smaller than those of Types I, II, and III in the whole range of W/L. This is mainly due to the increased added mass induced by the water body confined between the flexible curtains, which will be further discussed in Section 3.2.2.

The variation in pitch RAOs versus W/L for four types under three wave heights is plotted in Fig. 12. It is observed that the pitch RAO increases first and then decreases after reaching a peak with the increase in W/L for each specified type of breakwater and H_i. The pitch RAO of each specified type breakwater falls with the increase in the H_i, which is also reported by Ji et al. (2017) and Nasri et al. (2021). Through comparative analyses for four types of floating breakwater, it can be concluded that for all H_i, the peak values of the pitch RAOs of Types I and II are at the same level, larger than those of Types III and IV, and the peak value for Type III is the smallest among the four types of breakwater. From a holistic perspective, there is a surprising phenomenon that for Types I and II that lack the flexible component, the peaks of C_d and pitch RAO all occur at nearly the same W/L (see Figs. 9 and 12). This suggests a potential positive correlation between the pitch motion and wave power dissipation. In contrast, for Types

III and IV that own flexible components, the W/L corresponding to the peak of C_d is larger than that corresponding to the peak of pitch RAO. This discrepancy may be attributed to the buffer effect induced by the oscillation of the flexible curtains.

Moreover, the wave frequency corresponding to the maximum pitch RAO of Types I, II, III, and IV decreases in turn, occurring at $W/L = 0.34, 0.29, 0.29$, and 0.21, respectively, and the peak positions are found to be independent of the change of H_i. For this phenomenon, we consider that the addition of one underhanging component, either a rigid slotted barrier or a flexible curtain, increases the added mass of the breakwater and leads to a slight reduction in the natural frequency, intuitively embodied in the pitching resonant frequency. When two flexible curtains are mounted, the downward shift in pitching resonant frequency becomes more pronounced due to the increased added mass caused by the trapped waters between them. Furthermore, the motion damping is strengthened as well for its flexible characteristics and the slotted configuration can augment this effect further (Huang et al., 2014; Nasri et al., 2021).
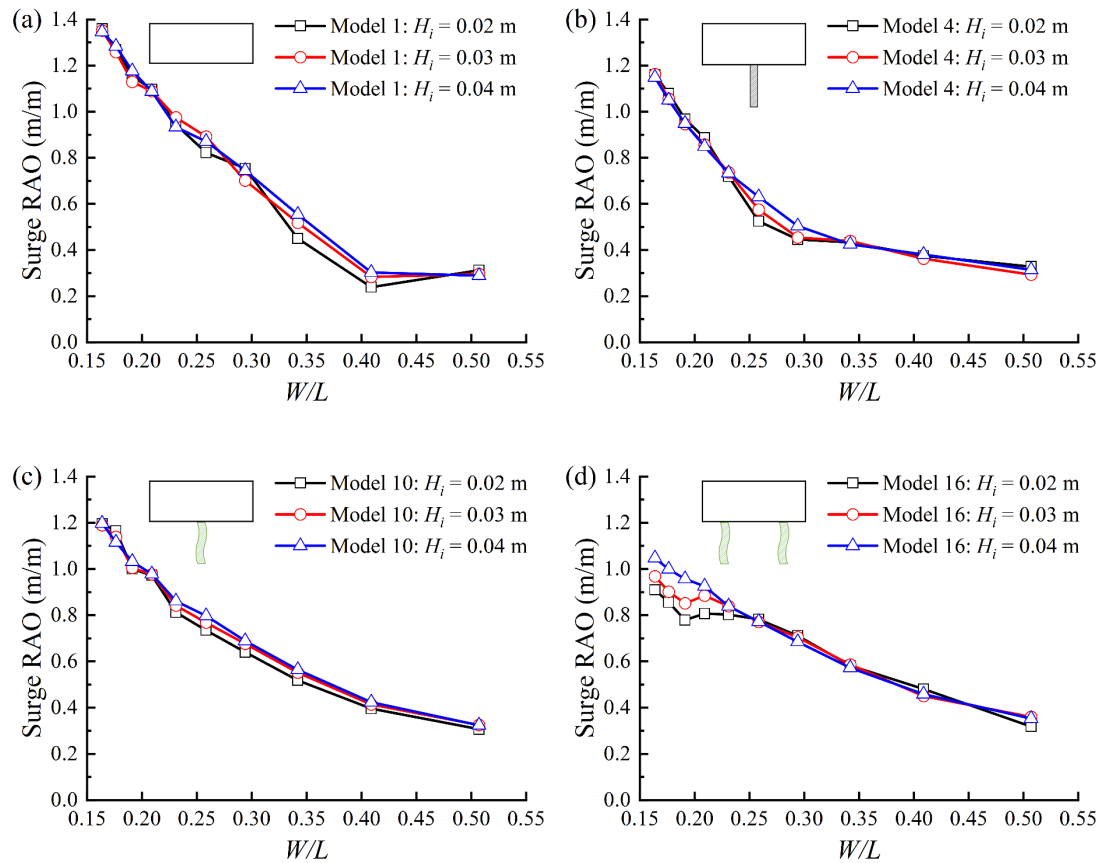
Fig. 10 Variation in surge RAOs versus W/L under three wave heights: (a) Type I; (b) Type II; (c) Type III; (d) Type IV.
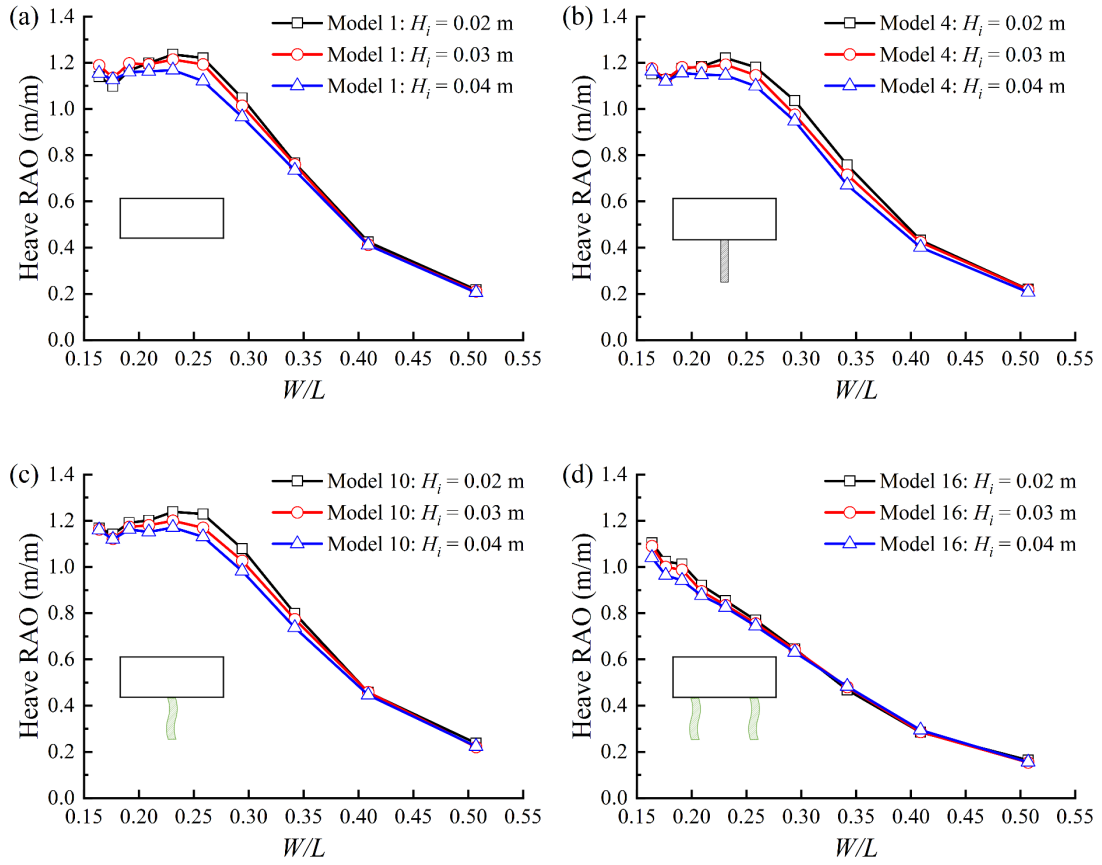
Fig. 11 Variation in heave RAOs versus *W/L* under three wave heights: (a) Type I; (b) Type II; (c) Type III; (d) Type IV.
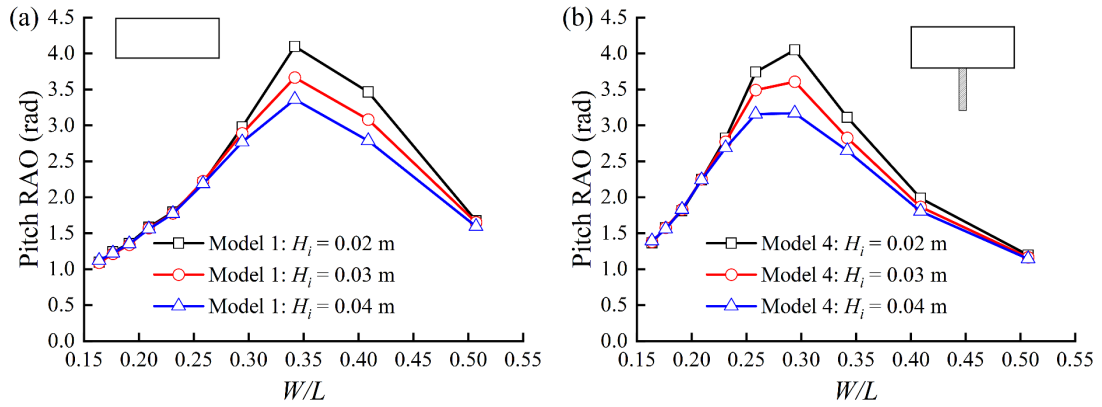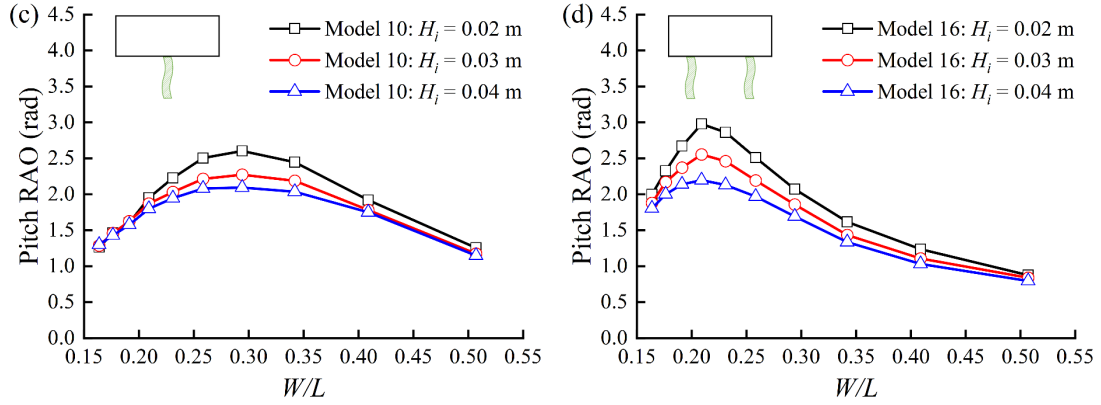
Fig. 12 Variation in pitch RAOs versus *W/L* under three wave heights: (a) Type I; (b) Type II; (c) Type III; (d) Type IV.

3.1.3. Seaward and leeward mooring forces

Figs. 13 and 14 illustrate the variations in the seaward and leeward normalized mooring forces, respectively, as a function of *W/L* for four types under three wave heights. Generally speaking, the seaward mooring force is larger than leeward, imposing higher load-bearing requirements on the mooring chain.

In Fig. 13, it is evident that a greater H_i consistently gives rise to a larger normalized seaward mooring force across all *W/L*, except Type IV at medium-period waves ($0.23 < W/L < 0.29$). This means that accompanying the increase in the wave height, the mooring force on the breakwater rises non-linearly. This in turn induces an enhanced obstruction of breakwater movement, which provides an explanation for the decrease in motion RAO observed with an increase in H_i. Moreover, it is observed that there is a dramatic rise of normalized seaward mooring force at $W/L < 0.41$ when $H_i = 0.04$ m for Types II and III, which may be because the mooring chain approaches the taut state. In the transition of the mooring chain from the slack state to the taut state, the mooring force will increase sharply. As compared to Type I, it is found that the addition of one underhanging component significantly augments seaward mooring force, especially when $H_i = 0.04$ m. When $H_i = 0.04$ m, the normalized seaward mooring force of Types II and III are two and half times and twice as large as is of Type I at $W/L = 0.26$, respectively, and reach their maximum value. When attaching the underhanging component, the wave-bearing area of the floating breakwater is enlarged, exposing the floating breakwater to larger wave forces (Sun et al., 2022). In addition, this phenomenon suggests that the amplification of the normalized seaward mooring force caused by attaching the rigid slotted barrier can be weakened by replacing it with a flexible curtain. Moreover, under this specified wave condition, this amplification is

counteracted when attaching two flexible curtains, that is to say, the normalized seaward mooring force of Type IV equals that of Type I approximately. As discussed in Section 3.1.2, the motion of breakwater motion is damped by attaching two flexible curtains, which will diminish the reliance of breakwater on the mooring system and decrease the seaward mooring force (Tang et al., 2011). It is also noteworthy that the reduction of the seaward mooring force by attaching two flexible curtains does not come at the expense of wave attenuation performance (see Fig. 8). As shown in Fig. 14, the H_i has a negligible effect on the normalized leeward mooring force of Type I, while the larger the H_i, the smaller the leeward mooring forces for Types II and III when W/L < 0.26. However, a greater H_i generally results in a larger normalized leeward mooring force of Type IV when W/L < 0.34. The leeward mooring forces of Types I and III decrease monochromatically with the increase in W/L, whereas the leeward mooring force of Type II is nearly constant when W/L > 0.34. The comparison of leeward mooring force among Types I, II, and III shows that the leeward mooring forces of Type II and Type I are minimum and maximum, respectively, among the three types in the whole range of W/L except W/L = 0.51, where the leeward mooring forces are almost the same for those three types of breakwater. Furthermore, the difference in leeward mooring force between Types I and IV is slight when W/L > 0.26, yet the leeward mooring force of Type IV tends to stay at a relatively steady level when W/L < 0.26, rather than continues to increase as W/L decreases like that of Type I. Meanwhile, the normalized leeward mooring force of Type IV varies in a narrow range, roughly between 0.0001 and 0.0008.
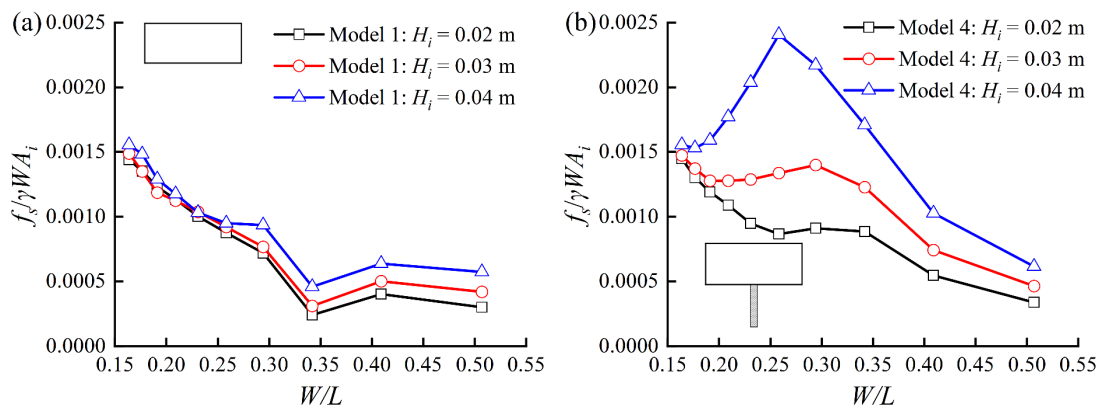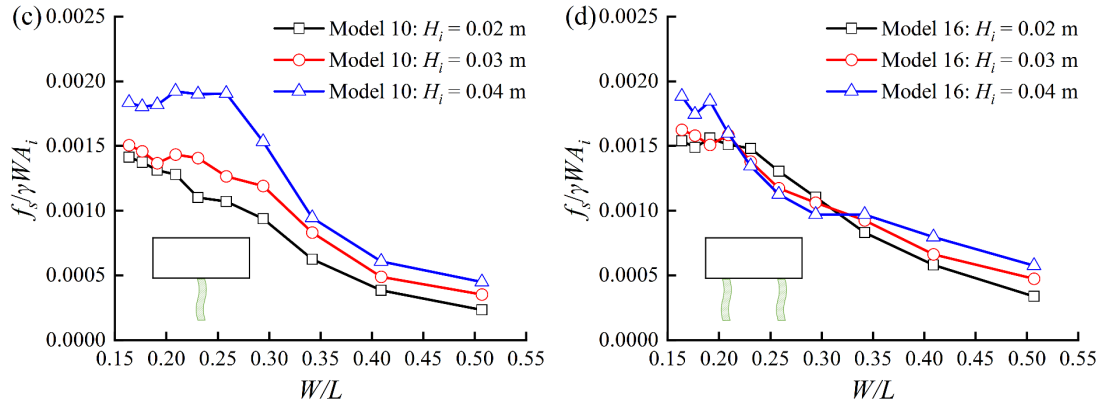
Fig. 13 Variation in normalized seaward mooring force versus *W/L* under three wave heights: (a) Type I; (b) Type II; (c) Type III; (d) Type IV.
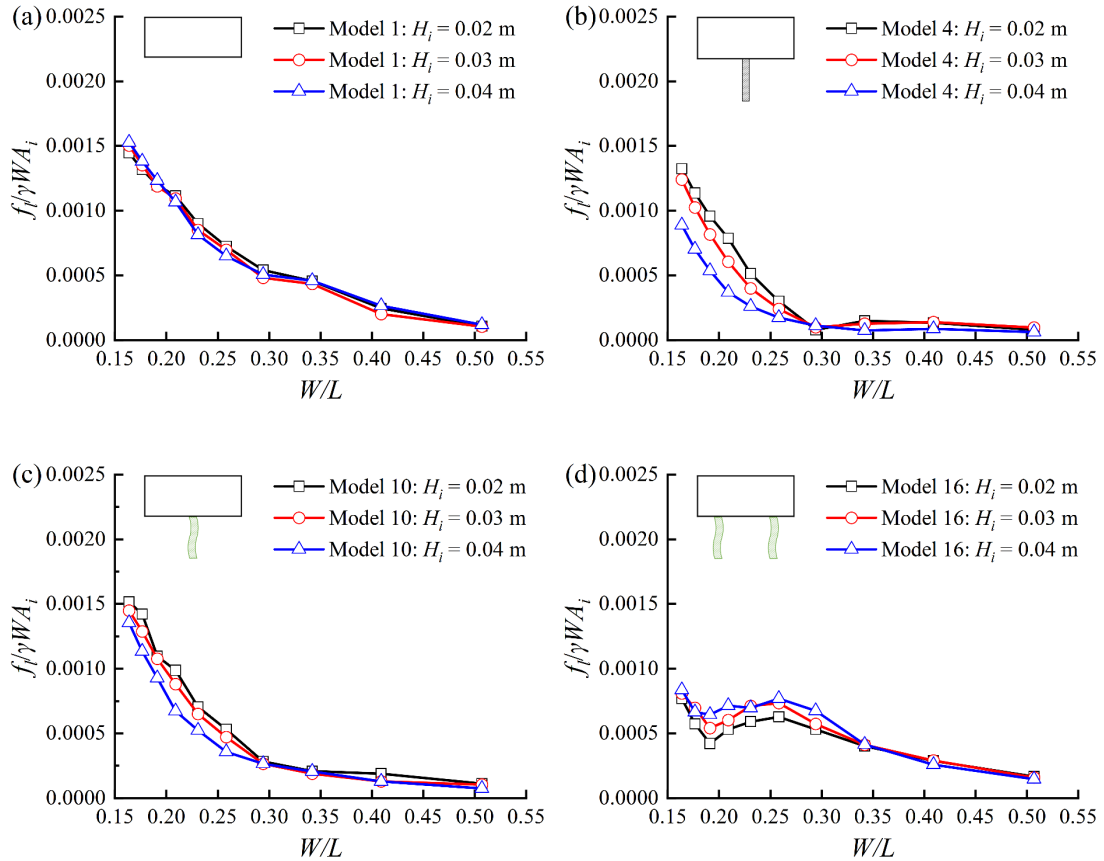

Fig. 14 Variation in normalized leeward mooring force versus *W/L* under three wave heights: (a) Type I; (b) Type II; (c) Type III; (d) Type IV.

3.2. Effects of the hanging length

Three hanging lengths of the underhanging component (*l* = 93, 163, and 233 mm) are selected to investigate their effect on the hydrodynamic performance of Types II, III, and IV of the floating breakwater. In this sub-section, the porosity of the

underhanging component and the wave height are fixed at 5.88% and 0.04 m, respectively.

3.2.1. Reflection, transmission, and wave power dissipation coefficients

Fig. 15 shows a comparison of C_r of three hanging lengths for Types II, III, and IV. The results indicate that increasing l can elevate C_r of Types II, III, and IV for short-period waves ($W/L > 0.41$), whilst the longest underhanging component yields the minimum of C_r when $W/L < 0.23$. Referring to $l = 93$ and 163 mm, the difference in C_r between Types II and III is mild in the whole range of W/L, whereas Type IV exhibits a larger C_r than Types II and III in almost the whole range of W/L.

Fig. 16 presents a comparison in C_t of three hanging lengths for Types II, III, and IV. It is found that increasing l from 93 mm to 163 mm enables a slight reduction and increase in C_t for Types II and III when $W/L < 0.34$ and $W/L > 0.41$, respectively. When increasing l to 233 mm, C_t of Types II and III notably descends in the whole W/L range, except for Types II in short waves ($W/L > 0.41$). For Type IV, when increasing l to 163mm, the minimum value of C_t decreases a lot to 0.11 (0.25 for $l = 93$ mm), and the corresponding W/L decreases as well. Additionally, C_t in long waves ($W/L < 0.29$) decreases significantly while increasing a little when $W/L > 0.34$. When increasing l to 233mm, the minimum value of C_t is nearly unchanged, which is 0.27, and its wave attenuation performance is enhanced across the entire range of W/L except 0.34. Additionally, compared to $l = 163$ mm, though it slightly underperforms for medium waves, its effective wave attenuation W/L range is enlarged because its long-wave attenuation is further enhanced. For any specified values of l, Type IV presents a larger C_t than Types II and III for short waves but the other way round for long waves.

The comparison in C_d of three hanging lengths for Types II, III, and IV is plotted in Fig. 17. The results show that the increase in l leads to a decrease and an increase in wave power dissipation, respectively, for short waves and long waves for Type IV of the breakwater. Similar results are also observed for Types II and III but with a rather small change of C_d at $W/L < 0.23$. For any specified l, Type IV performs much better than Types II and III in terms of wave power dissipation in long waves, and this advantage becomes increasingly prominent with the increase in l. Besides, the value of W/L that the maximum of C_d corresponds to decreases as l increases regardless of the type of the breakwater. Meantime, the maximum of C_d increases with the increase in l for Type II, while for Types III and IV, the maximum of C_d of $l = 163$ mm is the largest among the examined three values of l.
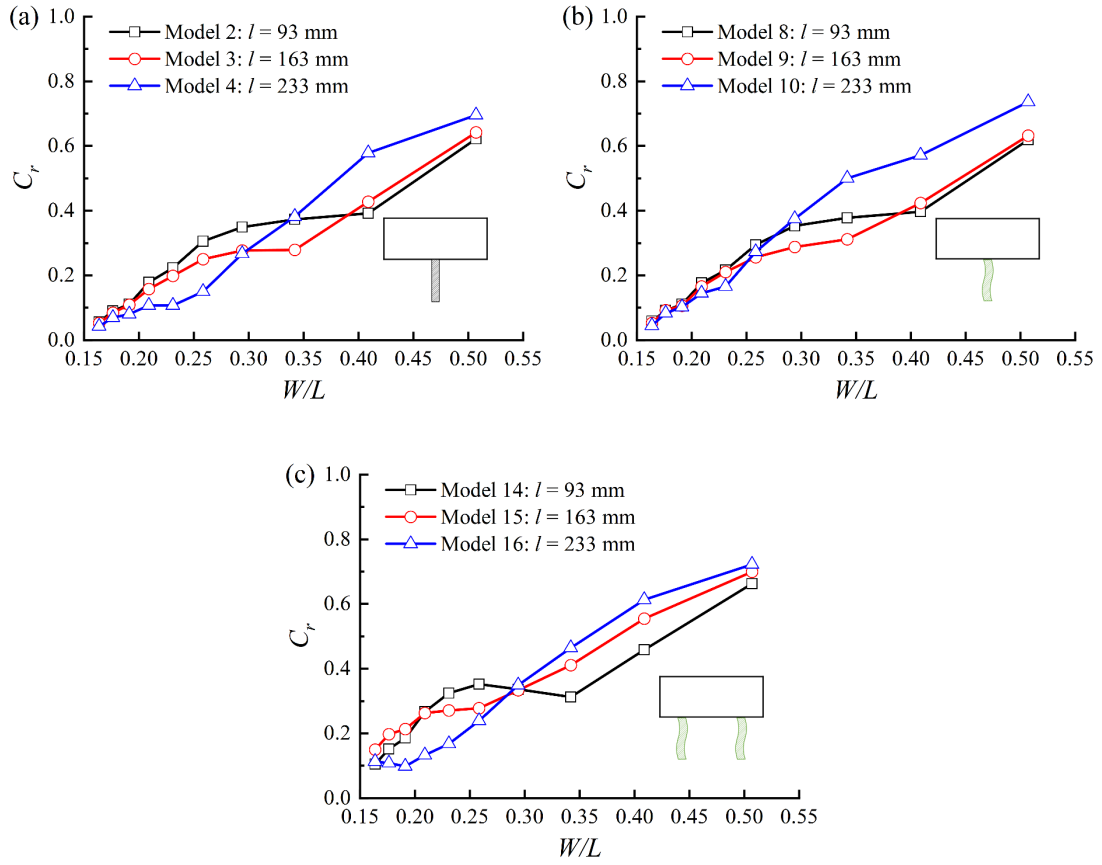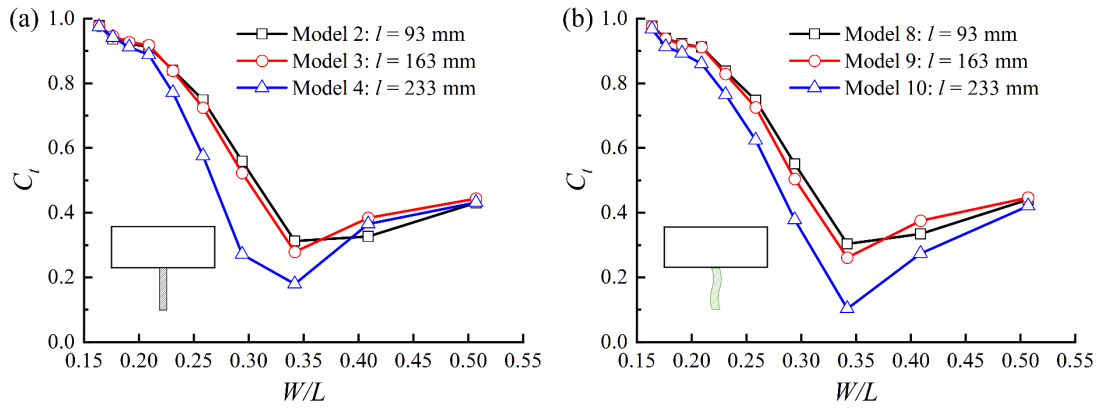
Fig. 15 Variation in reflection coefficient C_r versus W/L for three hanging lengths of underhanging component: (a) Type II; (b) Type III; (c) Type IV.
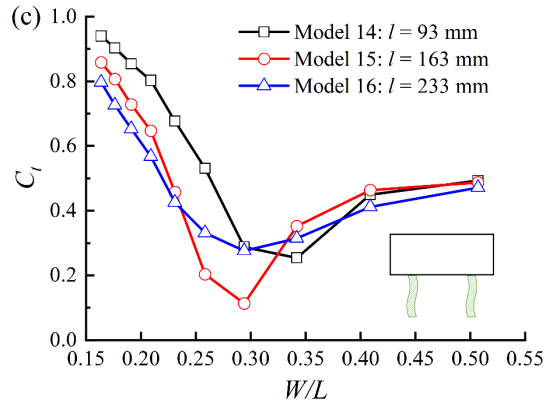
Fig. 16 Variation in transmission coefficient C_t versus W/L for three hanging lengths of underhanging component: (a) Type II; (b) Type III; (c) Type IV.
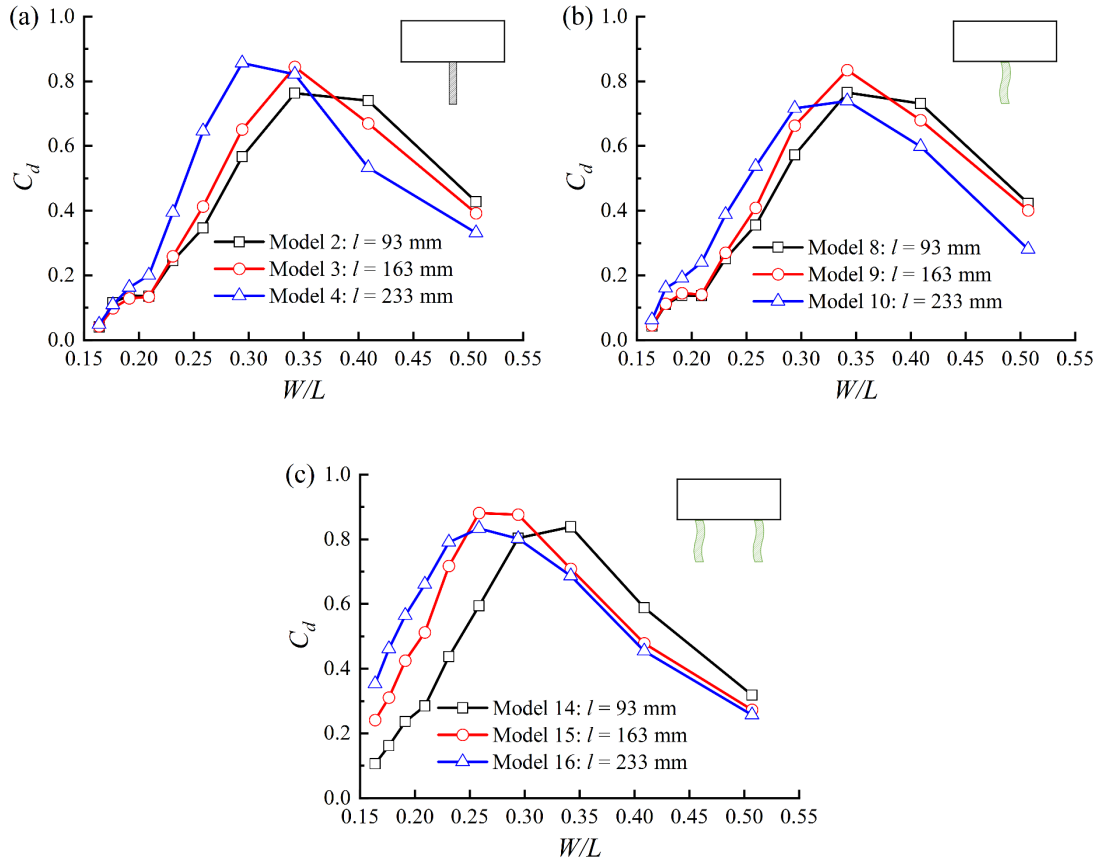

Fig. 17 Variation in wave power dissipation coefficient C_d versus W/L for three hanging lengths of underhanging component: (a) Type II; (b) Type III; (c) Type IV.

3.2.2. Surge, heave and pitch RAOs

The comparisons in surge, heave, and pitch RAOs of three lengths for Types II, III, and IV are shown in Figs. 18-20. Fig. 18 illustrates that for any specified l, the surge RAO decreases monochromatically with the increase in W/L regardless of the type of

the breakwater. The increase in l decreases the surge RAO in long waves for Types II and III when $W/L < 0.29$ and $W/L < 0.21$, respectively. For Type IV, the smallest surge RAO is achieved when the shortest curtain length $l = 93$ mm is used over $W/L > 0.26$.

The results plotted in Fig. 19 indicate that changing the hanging length has little effect on the heave RAO of Types II and III in the whole examined range of W/L, and the heave RAOs of those two types are nearly identical for any specified W/L. While for Type IV, the heave RAO is found to decrease significantly with the increase in l when $0.19 \leq W/L \leq 0.26$. For Types II and III, their heave RAOs both reach a value of 1.16 during the peak plateau states, with a corresponding threshold value of 0.26., regardless of the value of l. For Type IV with $l = 93$ mm, as W/L decreases, the heave RAO increases first and reaches the peak plateau state with the value of 1.20 when $W/L < 0.23$. Yet this peak plateau state is gone for the heave RAO of Type IV with $l = 163$ mm or 233 mm, and the heave RAOs of them decrease monochromatically with the increase in W/L.

Fig. 20 shows that the peak of the pitch RAO-W/L curve for Type IV becomes lower and moves towards low wave frequencies with the increase in l. Similar changes are also observed for Types II and III as l increases from 163 mm to 233 mm. Yet as l increases from 93 mm to 163 mm, the peak value of the pitch RAO for Types II and III nearly remains at the same level with the peak position slightly shifted towards low wave frequencies.

In general, with the increase in l, the motion damping and added mass are strengthened, the pitching resonant frequency shifts downward, and the long-wave attenuation performance is better. Meantime, the flexible damping effect becomes more evident for Types III and IV, and more water bodies are confined among the two flexible curtains for Types IV. Therefore, a noticeable downward shift of the pitching resonant frequency is observed. Moreover, the peak of pitch RAO is greatly decreased by lengthening the flexible curtain, especially when $l = 233$ mm. It is also noteworthy that the increased inertia moment due to the increase in l contributes to the reduction of pitch RAO as well.
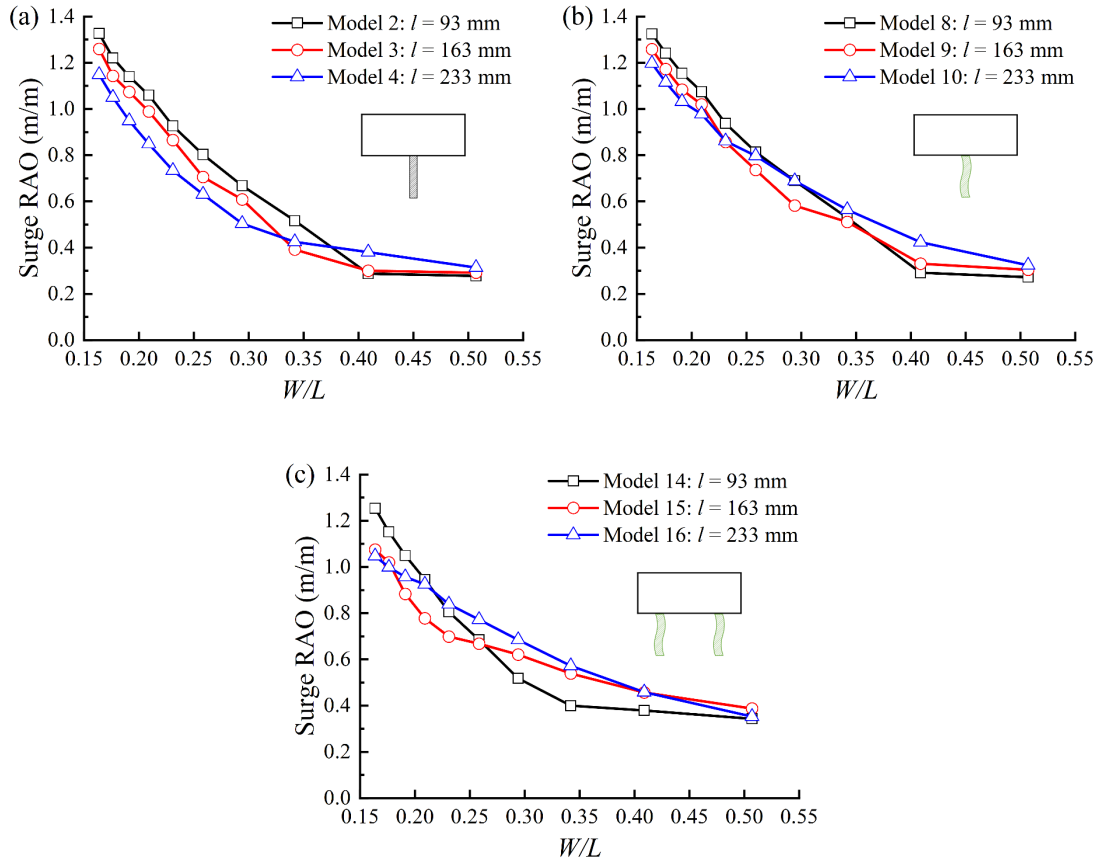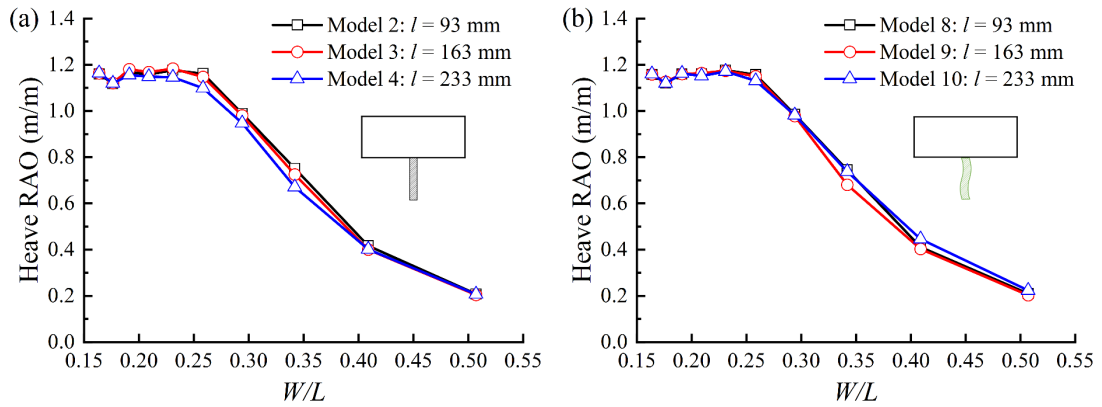
Fig. 18 Variation in surge RAOs versus *W/L* for three hang lengths of underhanging component: (a) Type II; (b) Type III; (c) Type IV.
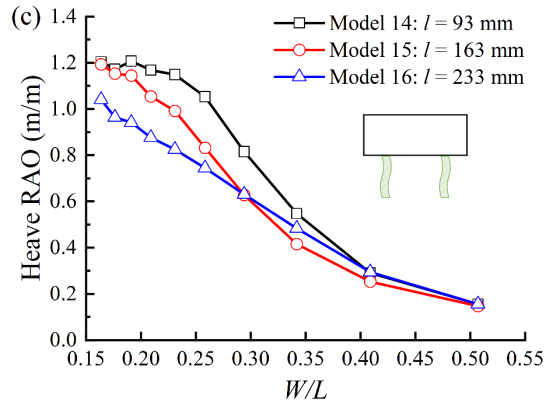
Fig. 19 Variation in heave RAOs versus *W/L* for three hanging lengths of underhanging component: (a) Type II; (b) Type III; (c) Type IV.
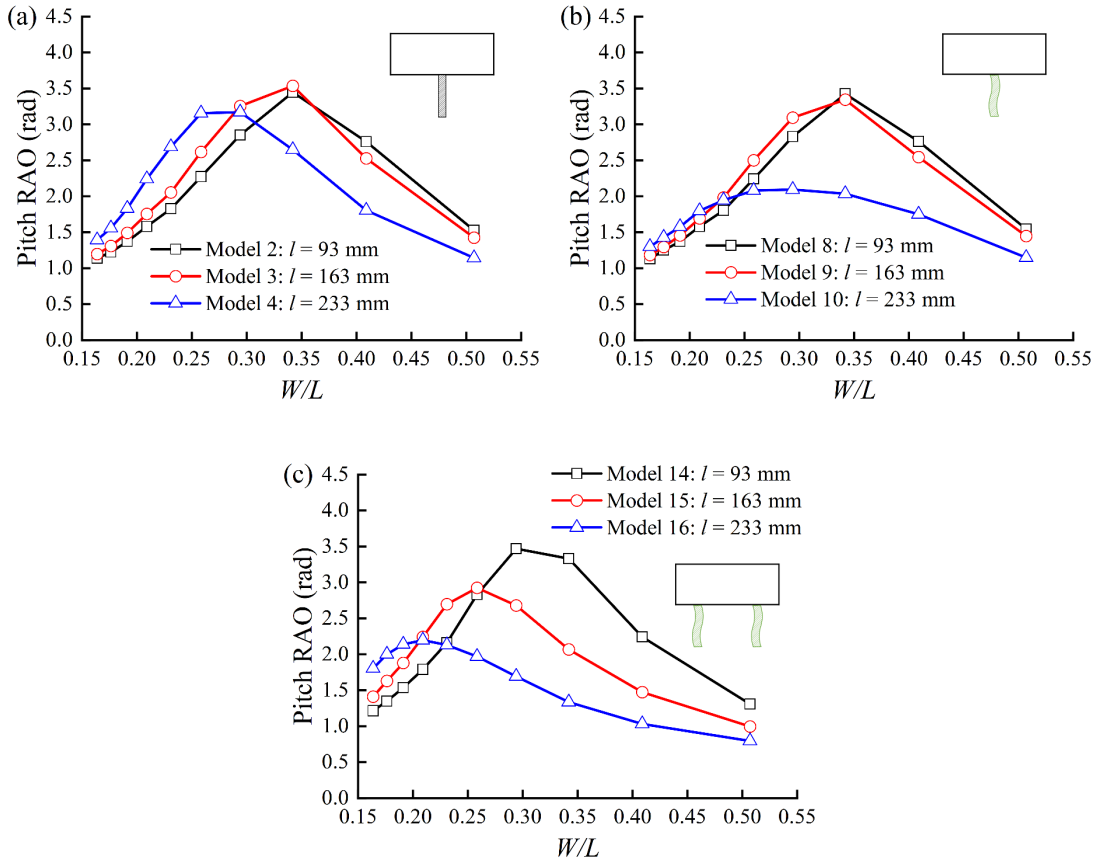

Fig. 20 Variation in pitch RAOs versus *W/L* for three hanging lengths of underhanging component: (a) Type II; (b) Type III; (c) Type IV.

3.2.3. Seaward and leeward mooring forces

Figs. 21 and 22 present comparisons in normalized seaward and leeward mooring forces, respectively, of three hanging lengths for Types II, III, and IV.

As shown in Fig. 21, the overall trend of the normalized seaward mooring force

generally shows a monotonic decline with the increase in W/L when l is small, say $l =$ 93 mm and 163 mm for all the examined types of breakwater. The overall monotonic decreasing trend is also observed when $l = 233$ mm for Type IV but not Types II and III, for which the normalized seaward mooring force rises dramatically at $W/L < 0.41$. Moreover, the peaks of the normalized seaward mooring force for Types II and III with $l = 233$ mm both occur at $W/L = 0.26$. Hence, when attaching one underhanging component, it is critical to consider both the wave attenuation performance and the load of the mooring chain while selecting its length. In terms of Type IV, this dramatic rise in the seaward mooring is overcome owing to the motion damping induced by the two flexible curtains.

Similar to the normalized seaward mooring force results, the normalized leeward mooring force as plotted in Fig. 22 also generally shows a monotonic decline with the increase in W/L except Type IV with $l = 233$ mm, for which a local peak occurs around $W/L = 0.26$. A larger l is found to result in a smaller normalized leeward mooring force for any specified wave condition for Types II and III. While for Type IV, conversely, the normalized leeward mooring force with $l = 233$ mm at $0.23 \leq W/L \leq 0.41$ is larger than those with $l = 93$ and 163 mm.
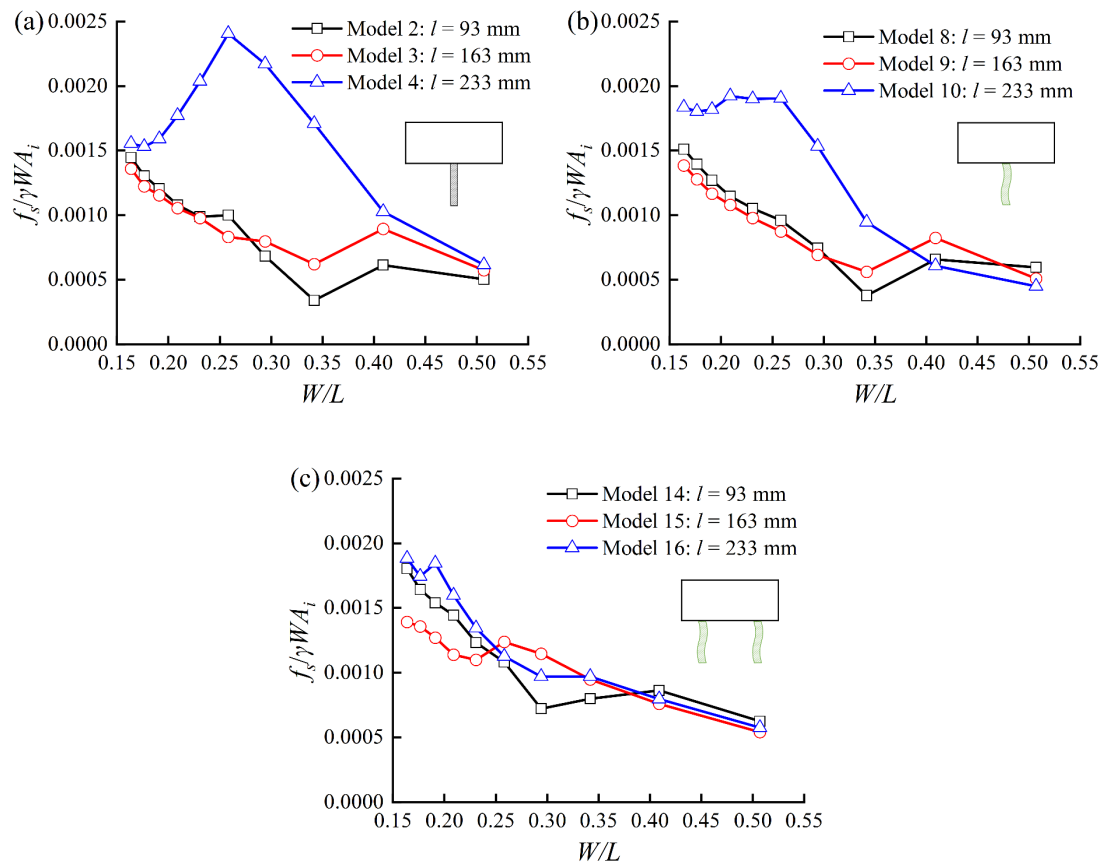

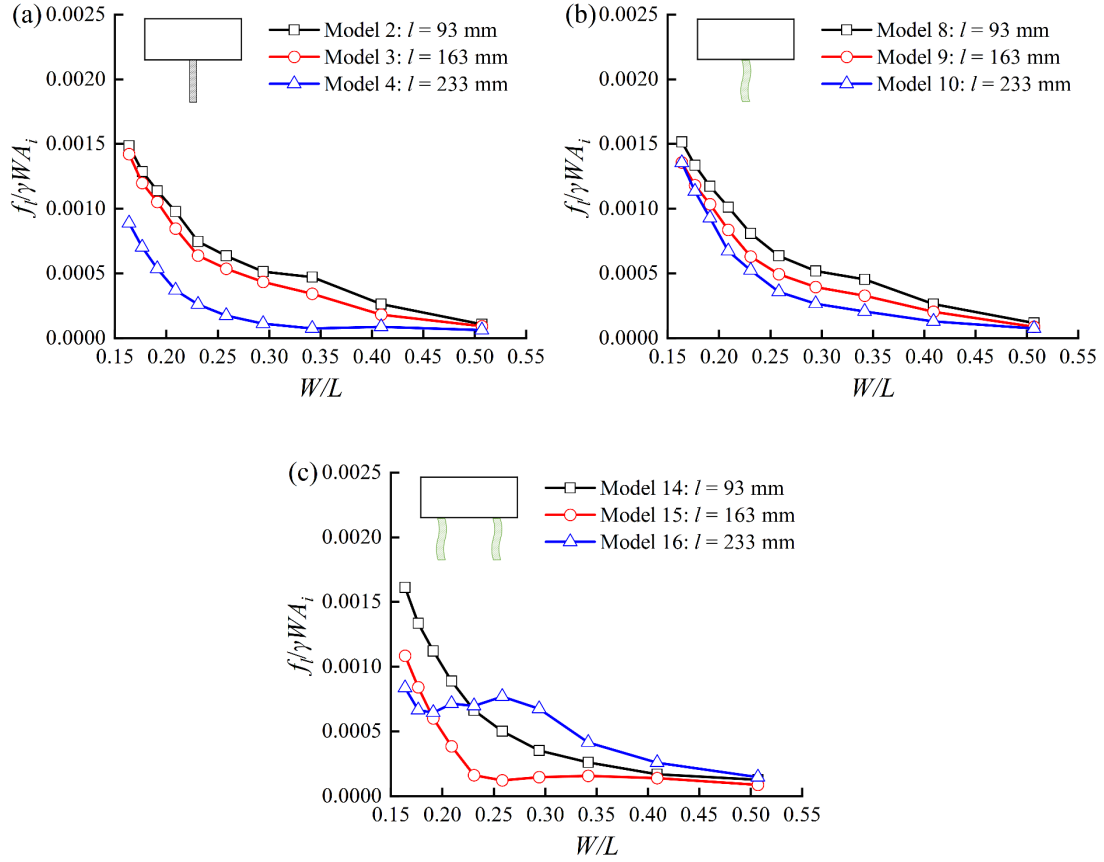Fig. 21 Variation in normalized seaward mooring force versus W/L for three hanging

Fig. 22 Variation in normalized leeward mooring force versus *W/L* for three hanging lengths of underhanging component: (a) Type II; (b) Type III; (c) Type IV.

3.3. Effects of the porosity

The effect of the porosity of the underhanging component on the hydrodynamic performance, including wave attenuation performance, motion responses, and mooring force, is investigated by examining four porosities for Types II, III, and IV. In this sub-section, the hanging length and the wave height are fixed at 233 mm and 0.04 m, respectively.

3.3.1. Reflection, transmission, and wave power dissipation coefficients

Fig. 23 presents a comparison in C_r of four porosities for Types II, III, and IV. For Type II, the effect of p on C_r varies with *W/L*: for wave conditions around $W/L = 0.25$, the larger the p, the larger the C_r; while for wave conditions at $W/L = 0.41$, a smaller C_r is obtained with the increase in p. For Type III, the influence of p on C_r mainly happens at short waves, e.g., $W/L > 0.34$, where C_r decreases with the increase in p. For Type IV, C_r is found to be insensitive to the change of p but $0.20 < W/L < 0.29$, where the largest C_r is obtained among the examined cases when the largest p, i.e., $p = 41.18\%$, is adopted.

28

Fig. 24 shows a comparison in C_t of four porosities for Types II, III, and IV. As illustrated in Figs. 24a and 24b, C_t slightly increases with the increase in p when 0.21 < W/L < 0.34 for Type II, and 0.19 < W/L < 0.39 for Type III. The minimum of C_t is found to occur at the W/L=0.34 for Types II and III regardless of the change of p. With regard to Type IV, increasing p results in an increase in C_t when W/L < 0.23, which is also can be seen in the study of Ji et al. (2017) and Guo et al. (2022). The valley of the C_r-W/L curve falls and moves towards large W/L with the increase in p.

The results of C_d plotted in Fig. 25 show that the increase in p leads to a slight decrease in C_d at W/L = 0.26 and 0.29 for Type II breakwater and 0.19 $\leq W/L \leq$ 0.26 for Type III. As a comparison, C_d for Type IV is found to be much more sensitive to the change of p when W/L < 0.23, and it drops significantly as p increases from 5.88% to 41.18%. The peak position of the C_d-W/L curve for Type IV moves towards large W/L with the increase in p.
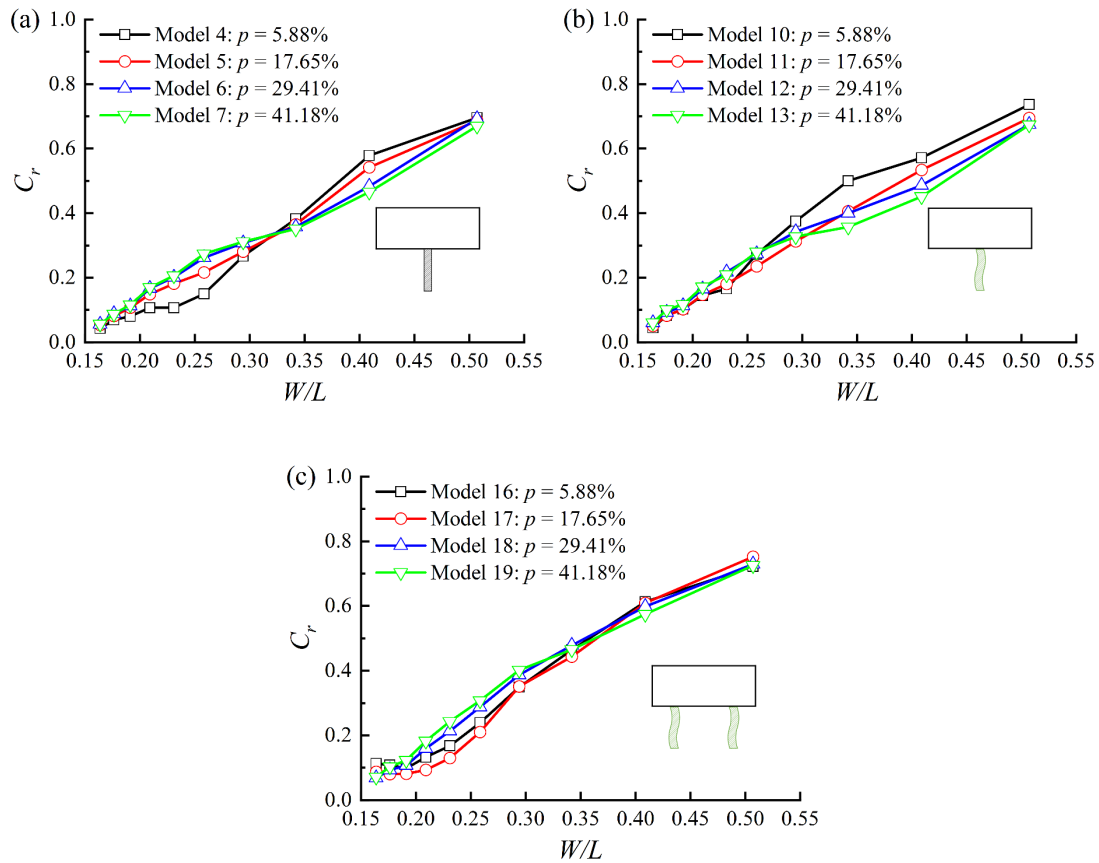

Fig. 23 Variation in reflection coefficient C_r versus W/L for four porosities of underhanging component: (a) Type II; (b) Type III; (c) Type IV.
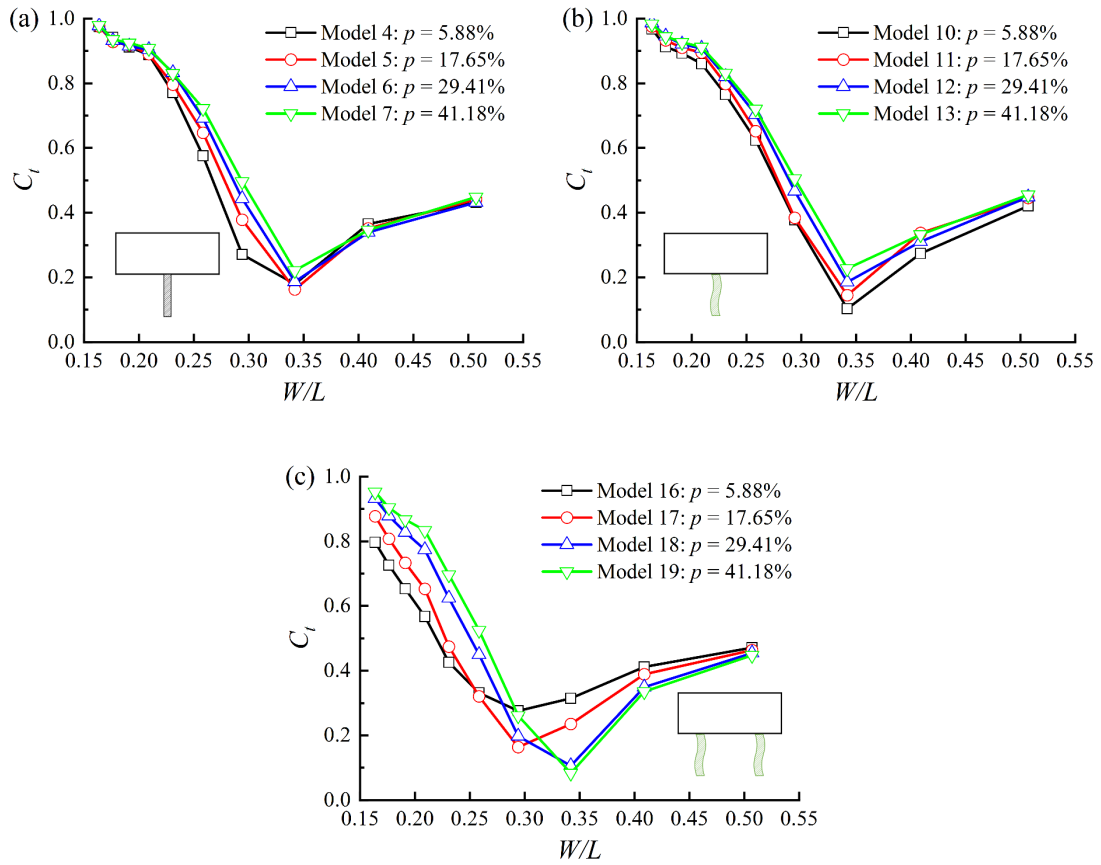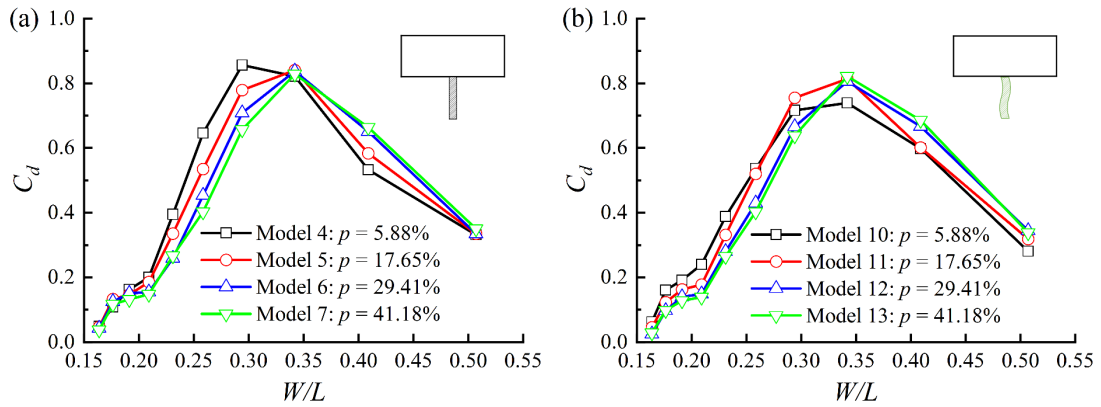
Fig. 24 Variation in transmission coefficient C_t versus W/L for four porosities of underhanging component: (a) Type II; (b) Type III; (c) Type IV.
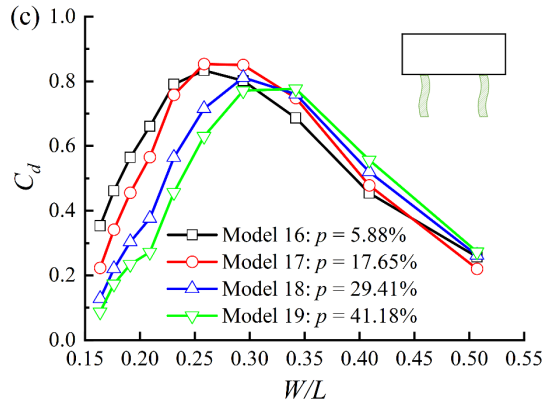
Fig. 25 Variation in wave power dissipation coefficient C_d versus W/L for four porosities of underhanging component: (a) Type II; (b) Type III; (c) Type IV.

3.3.2. Surge, heave and pitch RAOs

Figs. 26-28 present the results of surge, heave, and pitch RAOs with four porosities of the underhanging component for Types II, III, and IV. As shown in Fig. 26, no matter how p changes, the monotonic decreasing trend of the surge RAO - W/L curves for any type of the examined breakwaters remains unchanged. The surge RAO of Type II with $p = 5.88\%$ is much smaller than those with larger porosities when $W/L < 0.34$. For Type IV, the surge RAO with $p = 17.65\%$ is the smallest among the four examined porosities at long waves ($W/L < 0.23$). The surge RAO of Type IV at $0.29 \leq W/L \leq 0.41$, as well as that of Type III at $W/L = 0.41$, decreases with the increase in p.

As shown in Fig. 27, p is found to have a negligible effect on the heave RAOs of both Types II and III, whilst increasing p increases the heave RAO of Type IV in the whole range of W/L, especially for medium waves.

The results plotted in Fig. 28 show that the peak position of the pitch RAO-W/L curve moves towards short waves with the increase in p regardless of the types of the breakwater. The peak level for Type II first decreases and then increases whereas the peak level for Type III keeps rising as p increases from 5.88% to 41.18%. For short waves ($W/L \geq 0.34$), the larger the p, the larger the pitch RAO, and the pitch RAO of Type IV is the smallest one among the examined breakwaters for any specified p.

The decrease in the porosity exhibits a similar effect to increasing the hanging length of the underhanging component. Specifically, the damping effect and the effective mass of the rigid slotted barrier or flexible curtain, as well as the effective mass produced by the trapped water bodies between the two curtains, are enhanced with the decrease in p. As expected, the decrease in p can shift the pitching resonant frequency towards low frequencies, thereby enhancing the long-wave attenuation.

Furthermore, for Type IV, combined the threshold in *W/L* of the peak plateau state in the Figs. 11, 19, and 27, it is confirmed that a smaller *W/L* threshold for the peak plateau state of heave RAO can be obtained for a larger effective mass.
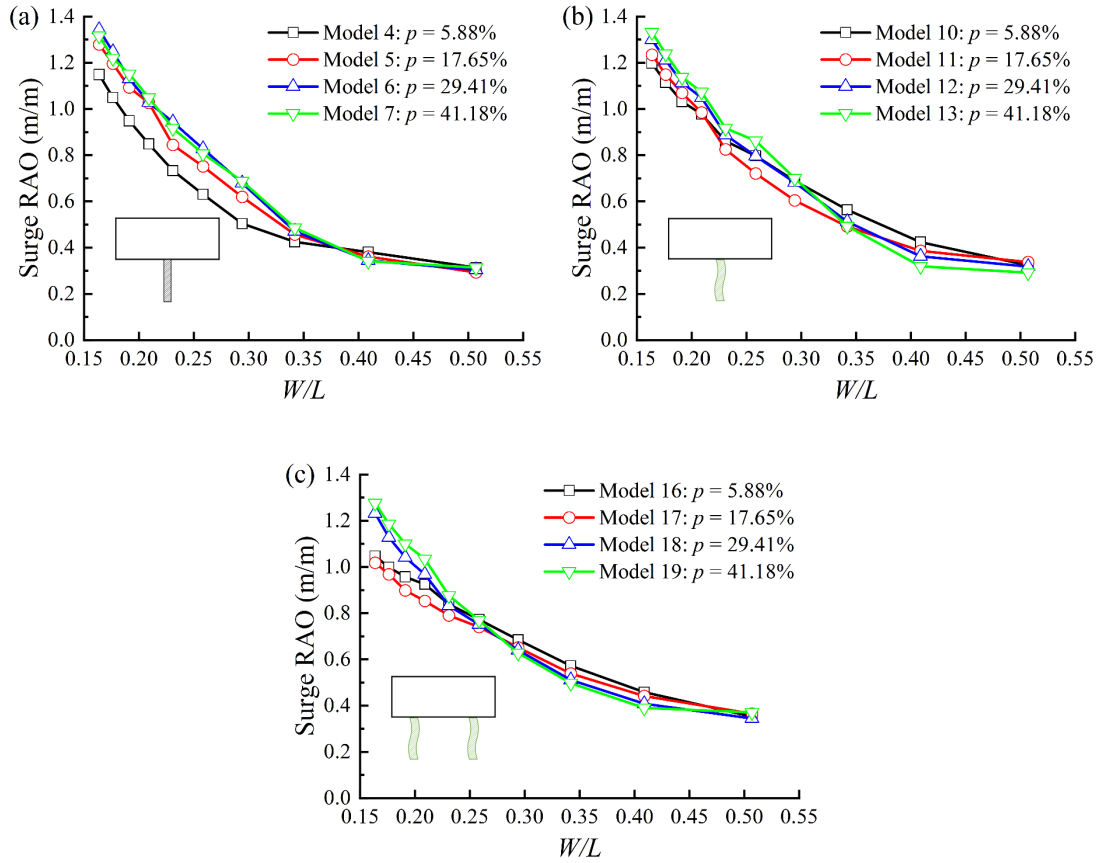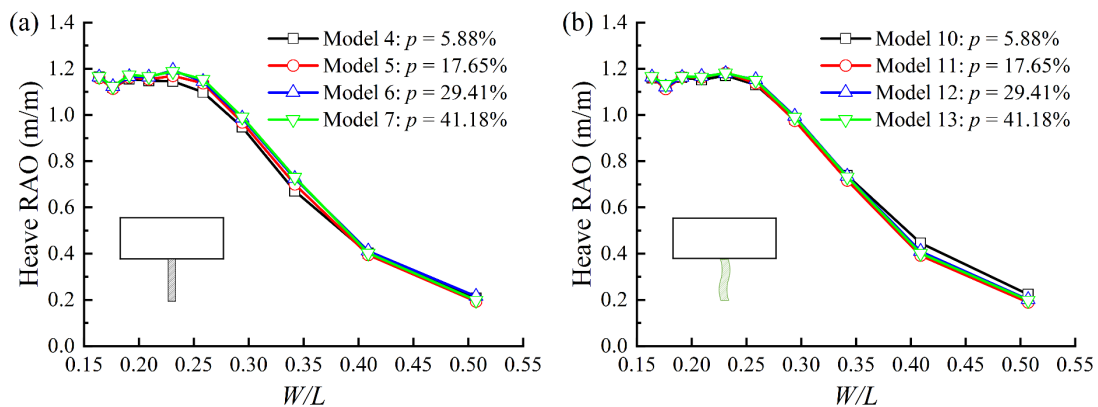

Fig. 26 Variation in surge RAOs versus *W/L* for four porosities of underhanging component: (a) Type II; (b) Type III; (c) Type IV.
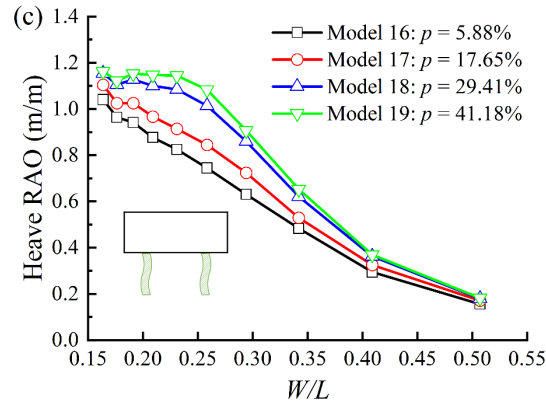
Fig. 27 Variation in heave RAOs versus *W/L* for four porosities of underhanging component: (a) Type II; (b) Type III; (c) Type IV.
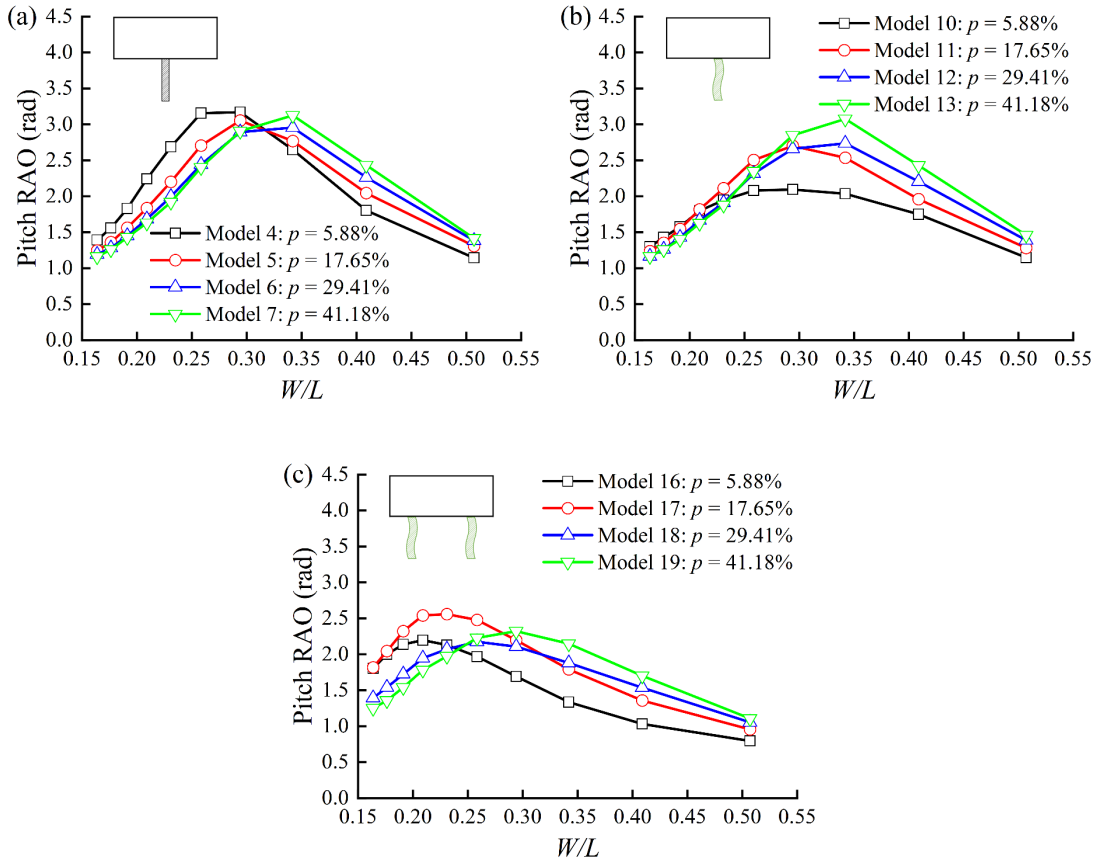

Fig. 28 Variation in pitch RAOs versus *W/L* for four porosities of underhanging component: (a) Type II; (b) Type III; (c) Type IV.

3.3.3. Seaward and leeward mooring forces

The variation in the normalized seaward and leeward mooring forces versus *W/L* are plotted in Figs. 29 and 30. As shown in Fig. 29a, the normalized seaward mooring force acting on Type II breakwater for $0.21 \leq W/L \leq 0.34$ with $p = 5.88\%$ can be

33

effectively damped by increasing p, and this change is particularly dramatic when p increases from 5.88% to 17.65%. A similar phenomenon also happens to the results of the normalized seaward mooring force acting on Type III breakwater for $W/L \leq 0.34$ (see Fig. 29b). As shown in Fig. 29c, there is no noticeable difference in the seaward mooring force of Type IV for different porosities of the curtains.

The results plotted in Fig. 30a show that the normalized leeward mooring force acting on Type II breakwater becomes larger as p increases for any specified value of W/L. Increasing p from 17.65% to 41.18% leads to a larger normalized leeward mooring force of Type III throughout nearly the whole range of W/L. However, the normalized leeward mooring force of Type IV for $p = 5.88\%$ is the largest at short and medium waves ($W/L \geq 0.23$). Regarding the underhanging component with p being 17.65%, 29.41%, and 41.18%, the difference in normalized leeward mooring forces between Types II and III is negligible. For $p = 29.41\%$ and 41.18%, the normalized leeward mooring force of Type IV is lower than that of both Types II and III in the whole range of W/L. For $p = 17.65\%$, Type IV exhibits a larger normalized leeward mooring force than both Types II and III at W/L ranging from 0.26 to 0.41, but a smaller one when $W/L < 0.23$.
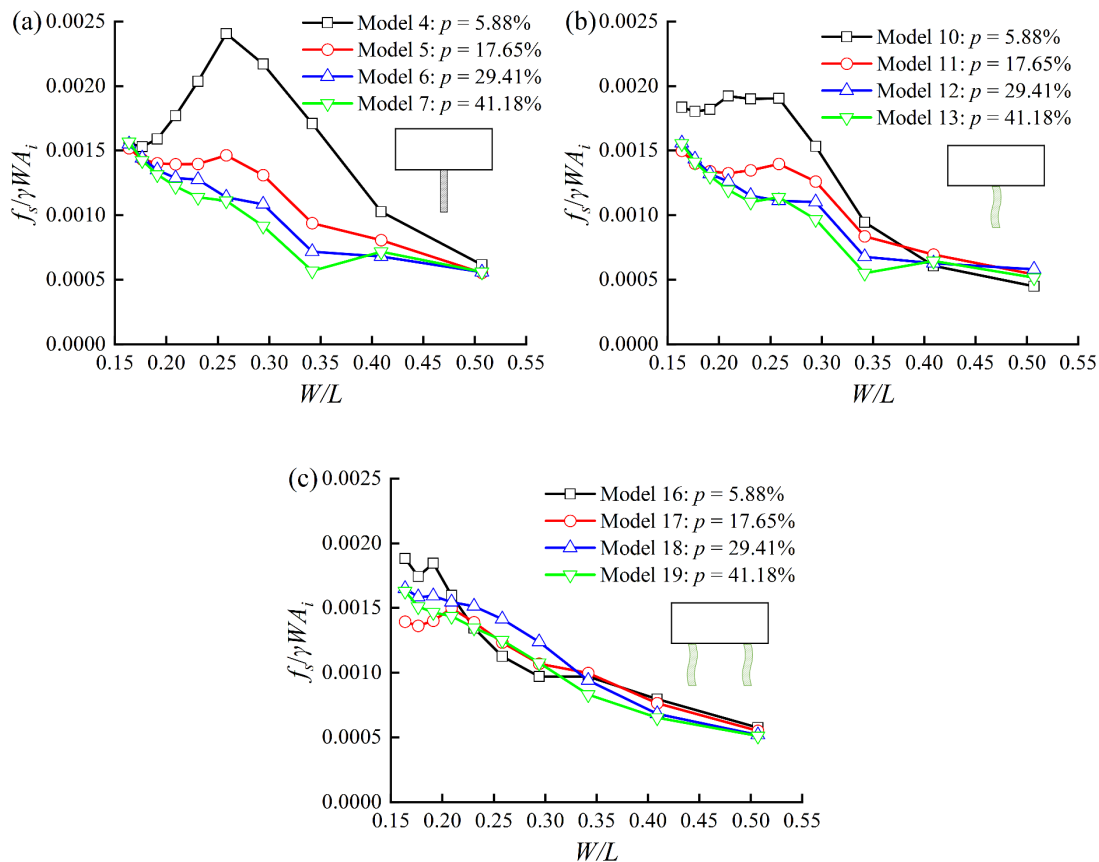

Fig. 29 Variation in normalized seaward mooring force versus W/L for four porosities
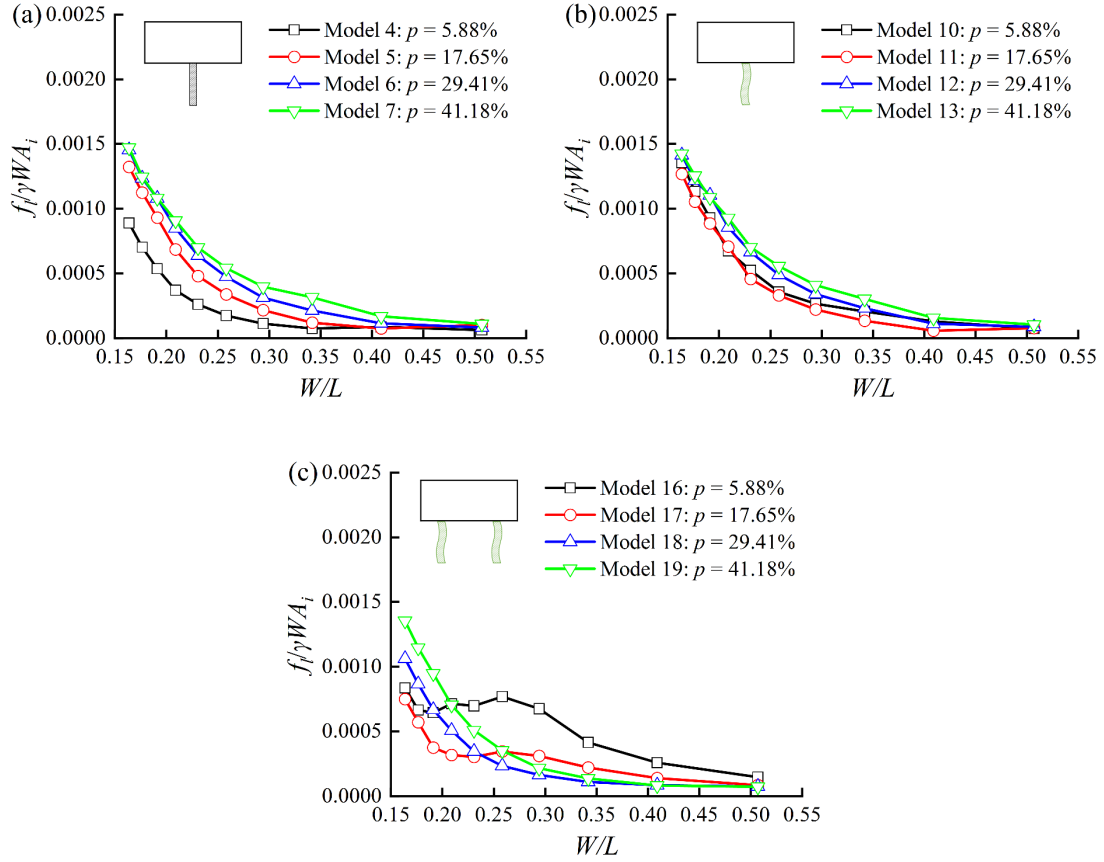
Fig. 30 Variation in normalized leeward mooring force versus W/L for four porosities of underhanging component: (a) Type II; (b) Type III; (c) Type IV.

3.4. Comparison of transmission coefficient C_t

A further detailed comparison of C_t is conducted with various types of floating breakwaters (shown in Fig.31), including floating box with horizontal plates (Han and Dong, 2023), floating box with truss structures (Uzaki et al., 2011), dual cylindrical pontoons (Ji et al., 2016), mesh cage with rubber bodies (Ji et al., 2016), dual cylindrical pontoon with nets (Ji et al., 2017) and floating box with pneumatic chambers (Howe et al., 2020). Models 15 and 16 in the present study are specifically selected for comparison. The wave protection performance of floating breakwaters is significantly influenced by wave characteristics, model width (W), draft (Dr), and mooring system. Table 4 provides specific parameters for each type of floating breakwater involved in the comparison. H_i/L, h/L, and H_i/h are commonly used to describe wave characteristics. Other specific parameters (Dr/h, the horizontal plate length L_w, the truss length a, the net length d_{net}, the power take-off damping of pneumatic chamber LDV_1) are also detailed in Table 4. Regarding W, if additional structures laterally extend the breakwater,

W refers to the total width of the main floating body and additional structures. For instance, *W* for a floating box with horizontal plates includes the main floating body and two horizontal plates. The effect of *W* can be evaluated by *W/L*, serving as the horizontal coordinate. It is noteworthy that all types of floating breakwaters involved in comparison are equipped with slack mooring systems. The attachment of horizontal plates or truss structure to the floating box enhances wave attenuation by boosting vortex shedding. The floating box with a pneumatic chamber adopted the oscillating water column wave energy conversion mechanism to attenuate wave energy. With the pneumatic damping effect, the motion response can be weakened. For dual cylindrical pontoon and mesh cage with rubber bodies, they can increase the moment of inertia and the water sloshing inside the gap also can boost wave energy dissipation. Ji et al. (2017) also recognized the beneficial effect of flexible materials in wave protection. However, their performance was not significantly enhanced because the nets used were not elastic and had large porosity. Compared to these floating breakwaters, the rectangular floating breakwater with two flexible curtains as wave-dissipating components is particularly effective in attenuating waves, especially when interacting with medium and long waves.
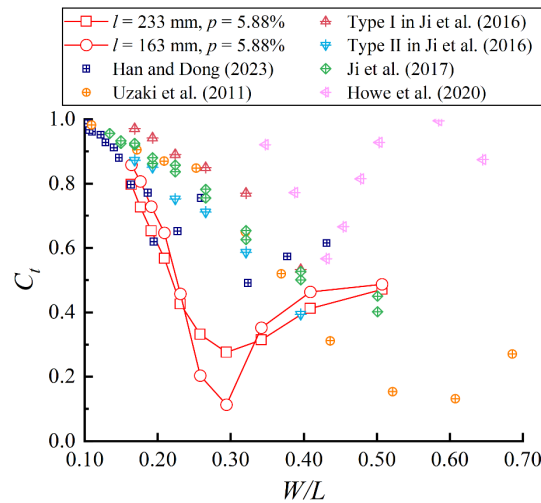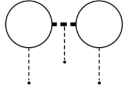

Fig. 31 Comparison of transmission coefficient C_t between the present study and other studies

Table 4. The test conditions involved in the comparison

Study	Configuration	H_i/L	h/L	H_i/h	Other parameters
The present study (box with flexible curtains)		0.013-0.040	0.131-0.406	0.10	$Dr/h = 0.325$, $p = 5.88\%$, $l = 0.163$, 0.233 m
Han and Dong (2023) (box with horizontal plates)		0.014-0.065	0.092-0.431	0.15	$Dr/h = 0.3$, $L_w = 0.05$, 0.10, 0.15 m
Uzaki et al. (2011) (box with truss structure)		0.029-0.059	0.136-1.224	0.04-0.21	Body width is 0.36 m, $Dr/h = 0.1$, $a = 0.12$ m
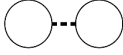
Ji et al. (2016) (I: cylindrical pontoons; II: Mesh cage with rubber bodies)	⃝--⃝	0.051-0.119	0.337-0.792		$Dr/h = 0.1$
	▭	0.051-0.119	0.337-0.792	0.15	
Ji et al. (2017) (cylindrical pontoon with nets)	⃝--⃝	0.027-0.100	0.268-1.001	0.10	$Dr/h = 0.1$, $p = 60\%$, $d_{net} = 0.25, 0.35$ m
Howe et al. (2020) (box with pneumatic chamber)	▭	0.006-0.018	0.174-0.555	0.03	$Dr/h = 0.5$, $W = 1.2$ m LDV_1 damping
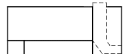
To directly illustrate the advantages of the rectangular floating breakwater with flexible curtains within the four tested floating water, C_t of four types of floating breakwater under $H_i = 0.04$ m are shown in Fig. 32. For types II, III, and IV, $l = 233$ mm and $p = 5.88\%$. All types of floating breakwaters demonstrate effective wave attenuation for short waves. When $W/L < 0.30$, the type IV floating breakwater exhibits the smallest C_t due to its large natural period. Remarkably, the type IV floating breakwater maintains a C_t lower than 0.5 when $W/L > 0.20$, showcasing its exceptional wave protection performance.
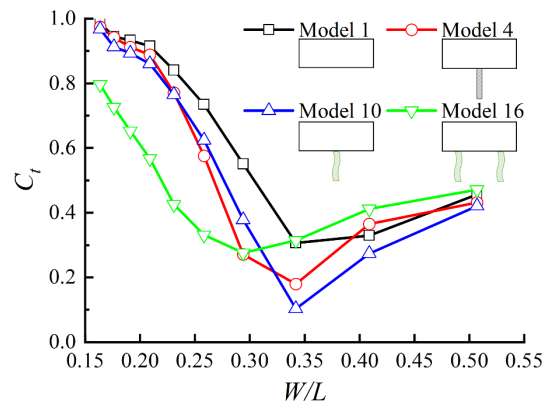

Fig. 32 Variation in transmission coefficient C_t versus W/L for four types of floating breakwater.

4. Conclusions

A rectangular floating breakwater with flexible curtains as wave-dissipating components was investigated experimentally to demonstrate how the curtain's different attributes impact the hydrodynamic performance of the floating breakwater. Apart from the rectangular breakwater with flexible curtains, the performances of the stand-alone rectangular floating breakwater and the one equipped with an attached rigid slotted barrier are also examined for comparison in our study. According to the experimental

study, the following key conclusions can be drawn:

1) Due to the non-linear enhancement of vortex-induced dissipation with the increase in wave height, increasing wave height tends to result in enhanced wave attenuation. However, in the case of a floating breakwater with two flexible curtains exposed to medium waves, the curtains' trapped effect on large wave heights is comparatively weak, hence the effect of increasing the wave height is the opposite.

2) The flexible curtains are proven to be effective wave-dissipating components for rectangular floating breakwaters, enhancing long-wave attenuation. The addition of one flexible curtain can induce an increase in the added mass, leading to a downward shift in the natural frequency of the floating breakwater. This effect is particularly pronounced when attaching two flexible curtains, as the confined water bodies among them significantly contribute to this phenomenon. Simultaneously, there is an enhancement in motion damping owing to the slotted structure and the buffer function of the flexible curtain, especially in heave and pitch motions. All of these mechanisms work together to enhance the dissipation of wave power when confronted with long waves.

3) With regard to the effect of increasing hanging length on wave attenuation, while the flexible curtain owns additional flexible features in contrast to the rigid slotted barrier, their effect is nearly the same when attaching one of them, facilitating the attenuation against waves across full test wave periods. Concerning attaching two flexible curtains, though the wave attenuation for medium waves may be diminished to some extent when the hanging length is relatively long, it owns superior long-wave attenuation. The effect of decreasing the porosity is similar to increasing the hanging length.

4) The rigid slotted barrier with both large length and low porosity can give rise to the excessive seaward mooring force for medium waves, which may result in a damage problem at the connection point between the floating breakwater and mooring chains. As an alternative to the rigid slotted barrier, the flexible curtain can be employed to mitigate and diminish the excessive load exerted on the seaward mooring chain described earlier. Installing two flexible curtains can help reduce the impact of excessive loads by dampening the motion of the breakwater caused by water waves.

In general, the supplement of two flexible curtains is a cost-effective way to improve the performance of the rectangular box-type floating breakwater, enhancing the long-wave attenuation without high demand for the mooring system. Although

systematic model tests are conducted on various scenarios of breakwaters, the number of tested devices in our experimental study remains limited. In the future, theoretical and numerical simulations can be carried out to study more scenarios, discussing the influence of more parameters, such as the impact of a greater number of underhanging components, on the performance of the floating breakwater. In addition, the flexible response of the flexible curtain also deserves future attention, which could help understand details of the trapped waves and be investigated by numerical simulation.

Acknowledgments

Appendix

Time histories of free surface elevations recorded by WG3-4, the mooring forces and the breakwater motion responses are presented in Fig. A1. The experimental test conditions are: Type IV, $l = 233$ mm, $p = 5.88\%$, $T = 1.1$ s, $H_i = 0.04$m. In Fig. A1(c), detrending involves eliminating a trend from the time histories, where a trend typically indicates a change in the mean over time. Regarding the surge motion of a floating breakwater, the amplitude of the surge motion remains stable after detrending, despite the presence of a slow drifting motion.
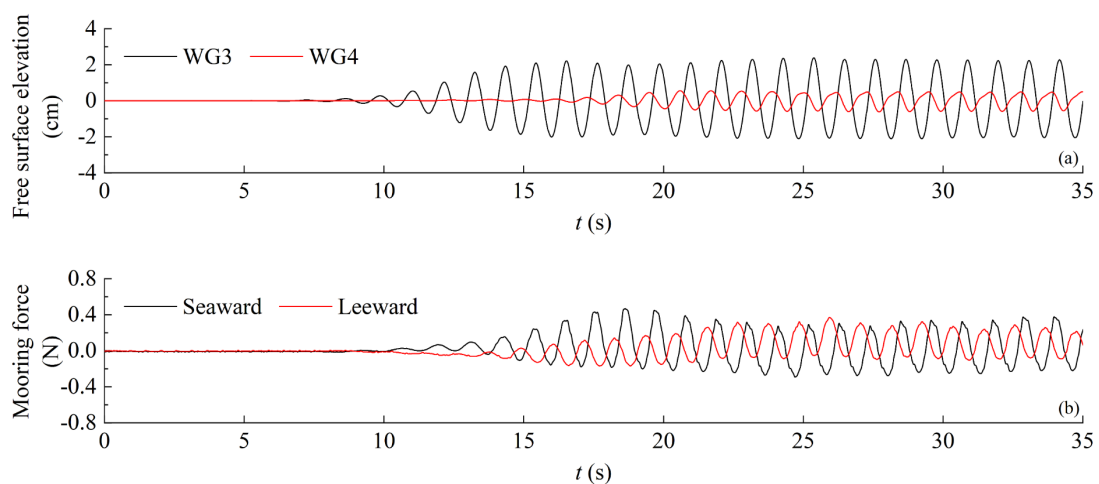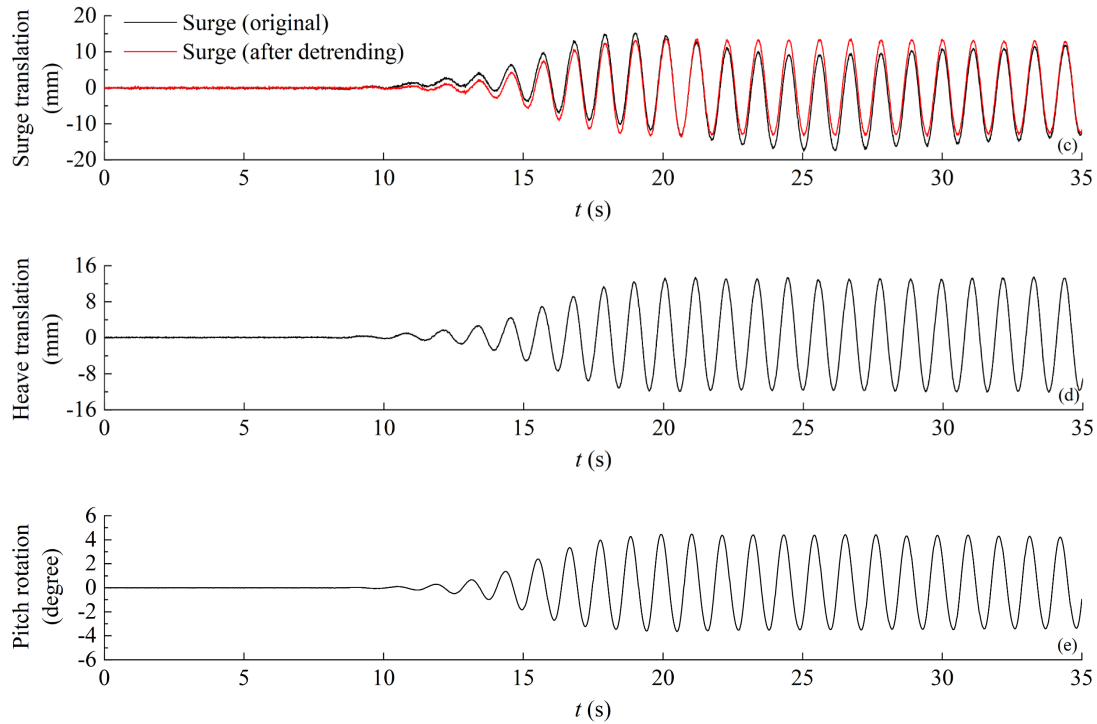
Fig. A1 Time histories of free surface elevations recorded by WG3-4, the mooring forces and the breakwater motion responses; the experimental test conditions are: Type IV, $l = 233$ mm, $p = 5.88\%$, $T = 1.1$ s, $H_i = 0.04$m.

References

Adee, B. H., 1976. Floating breakwater performance. In: Proceedings of the 15th Conference on Coastal Engineering, ASCE, Honolulu, HI, pp. 2777-2791.

Alamailes, A., Türker, U., 2019. Using analytical approach to estimate wave transmission coefficient in floating structures. J. Waterway, Port, Coastal, Ocean Eng. 145, 04019010.

Chanda, A., Bora, S. N., 2020. Effect of a porous sea-bed on water wave scattering by two thin vertical submerged porous plates. European Journal of Mechanics - B/Fluids. 84, 250-261.

Chanda, A., Pramanik, S., 2023. Effects of a thin vertical porous barrier on the water wave scattering by a porous breakwater. Phys. Fluids. 35, 062120.

Chen, J., Zhang, J., Wang, G., Zhang, Q., Guo, J., Sun, X., 2022. Numerical simulation of the wave dissipation performance of floating box-type breakwaters under long-period waves. Ocean. Eng. 266, 113091.

Cheng, Y., Fu, L., Dai, S., Collu, M., Ji, C., Yuan, Z., et al., 2022. Experimental and numerical investigation of WEC-type floating breakwaters: A single-pontoon oscillating buoy and a dual-pontoon oscillating water column. Coast. Eng. 177, 104188.

Cheng, Y., Ji, C., Gu, X., Huo, F., Cui, J., Yuan, Z., 2021. Hydrodynamics of a dual-module pontoon-net floating breakwater system: Numerical simulations and prototype tests. J. Hydrodyn. 33, 915-927.

Cho, I. H., Kee, S. T., Kim, M. H., 1997. The performance of flexible-membrane wave barriers in oblique incident waves. Appl. Ocean Res. 19, 171-182.

Dai, J., Wang, C. M., Utsunomiya, T., Duan, W., 2018. Review of recent research and developments on floating breakwaters. Ocean. Eng. 158, 132-151.

Deng, Z., Wang, L., Zhao, X., Huang, Z., 2019. Hydrodynamic performance of a T-shaped floating breakwater. Appl. Ocean Res. 82, 325-336.

Dong, G. H., Zheng, Y. N., Li, Y. C., Teng, B., Guan, C. T., Lin, D. F., 2008. Experiments on wave transmission coefficients of floating breakwaters. Ocean. Eng. 35, 931-938.

Drew, B., Plummer, A. R., Sahinkaya, M. N., 2009. A review of wave energy converter technology. Proceedings of the Institution of Mechanical Engineers, Part A: Journal of Power and Energy. 223, 887-902.

Falcão, A. F. O., Henriques, J. C. C., 2014. Model-prototype similarity of oscillating-water-column wave energy converters. Int. J. Mar. Energy. 6, 18-34.

Goda, Y., Suzuki, Y., 1976. Estimation of incident and reflected waves in random wave experiments. In: Proceedings of the 15th conference of coastal engineering, Honolulu, Hawaii., pp. 828-845.

Guo, Y. C., Mohapatra, S. C., Guedes Soares, C., 2022. Experimental study on the performance of an array of vertical flexible porous membrane type breakwater under regular waves. Ocean. Eng. 264, 112328.

Guo, Y. C., Mohapatra, S. C., Guedes Soares, C., 2023. An experimental study on the performance of combined membrane breakwaters against incident waves. Ocean. Eng. 280, 114793.

Hales, L. Z., 1981. Floating breakwaters: state-of-the-art literature review. Technical Report no. 81-1. US Army Engineer Waterways Experiment Station. Vicksburg, Mississippi, USA.

Han, X., Dong, S., 2023. Interaction between regular waves and floating breakwater with protruding plates: Laboratory experiments and SPH simulations. Ocean. Eng. 287, 115906.

He, F., Huang, Z., Law, A. W. K., 2013. An experimental study of a floating breakwater with asymmetric pneumatic chambers for wave energy extraction. Appl. Energy. 106, 222-231.

He, F., Leng, J., Zhao, X., 2017. An experimental investigation into the wave power extraction of a floating box-type breakwater with dual pneumatic chambers. Appl. Ocean Res. 67, 21-30.

He, F., Li, J., Pan, J., Yuan, Z., 2023. An experimental study of a rectangular floating breakwater with vertical plates as wave-dissipating components. Appl. Ocean Res. 133, 103497.

Howe, D., Nader, J.-R., Macfarlane, G., 2020. Experimental investigation of multiple oscillating water column wave energy converters integrated in a floating breakwater: Wave attenuation and motion characteristics. Appl. Ocean Res. 99, 102160.

Huang, Z., He, F., Zhang, W., 2014. A floating box-type breakwater with slotted barriers. J Hydraul Res. 52, 720-727.

Ji, C., Bian, X., Cheng, Y., Yang, K., 2019. Experimental study of hydrodynamic performance for double-row rectangular floating breakwaters with porous plates. Ships and Offshore Structures. 14, 737-746.

Ji, C., Bian, X., Xu, S., Guo, J., Huo, F., 2023. Numerical study on the hydrodynamic performance of floating breakwaters with complex configurations. Ocean. Eng. 273, 114032.

Ji, C., Chen, X., Cui, J., Gaidai, O., Incecik, A., 2016. Experimental study on configuration optimization of floating breakwaters. Ocean. Eng. 117, 302-310.

Ji, C., Cheng, Y., Cui, J., Yuan, Z., Gaidai, O., 2018. Hydrodynamic performance of floating breakwaters in long wave regime: An experimental study. Ocean. Eng. 152, 154-166.

Ji, C., Cheng, Y., Yang, K., Oleg, G., 2017. Numerical and experimental investigation of hydrodynamic performance of a cylindrical dual pontoon-net floating breakwater. Coast. Eng. 129, 1-16.

Jin, H., Zhang, H., Xu, D., Liu, C., Xu, S., 2022. Analytical investigation on wave attenuation performance of a floating breakwater with nonlinear stiffness. Ocean. Eng. 243,

Kim, M. H., Kee, S. T., 1996. Flexible-membrane wave barrier. I: Analytic and numerical solutions. J.

Waterway, Port, Coastal, Ocean Eng. 122, 46-53.

Koutandos, E., Prinos, P., Gironella, X., 2005. Floating breakwaters under regular and irregular wave forcing: reflection and transmission characteristics. J Hydraul Res. 43, 174-188.

Li, C., Zhang, H., Zhang, H., Sun, B., Yang, S., 2022. Wave-attenuation and hydrodynamic properties of twin pontoon floating breakwater with kelp. Appl. Ocean Res. 124, 103213.

Liang, J., Liu, Y., Chen, Y., Li, A., 2022. Experimental study on hydrodynamic characteristics of the box-type floating breakwater with different mooring configurations. Ocean. Eng. 254, 111296.

Liu, Z., Wang, Y., Wang, W., Hua, X., 2019. Numerical modeling and optimization of a winged box-type floating breakwater by Smoothed Particle Hydrodynamics. Ocean. Eng. 188, 106246.

McCartney, B. L., 1985. Floating breakwater design. J. Waterway, Port, Coastal, Ocean Eng. 111, 304-318.

Mohapatra, S. C., da Silva Bispo, I. B., Guo, Y., Guedes Soares, C., 2024. Analysis of Wave-Induced Forces on a Floating Rectangular Box with Analytical and Numerical Approaches. Journal of Marine Science and Application. 23, 113-126.

Murali, K., Amer, S. S., Mani, J. S., 2005. Dynamics of cage floating breakwater. J. Offshore Mech. Arct. Eng. 127, 331-339.

Murali, K., Mani, J. S., 1997. Performance of Cage Floating Breakwater. J. Waterway, Port, Coastal, Ocean Eng. 123, 172-179.

Nasri, B., Moghim, M. N., Badri, M. A., 2021. Experimental study on trapezoidal pontoon-type floating breakwaters with attached porous plates. J. Ocean Eng. Mar. Energy. 7, 41-57.

Ning, D., Zhao, X., Göteman, M., Kang, H., 2016. Hydrodynamic performance of a pile-restrained WEC-type floating breakwater: An experimental study. Renew Energ. 95, 531-541.

Qiao, D., Yan, J., Liang, H., Ning, D., Li, B., Ou, J., 2020. Analysis on snap load characteristics of mooring line in slack-taut process. Ocean. Eng. 196, 106807.

Rageh, O. S., Koraim, A. S., 2010. Hydraulic performance of vertical walls with horizontal slots used as breakwater. Coast. Eng. 57, 745-756.

Rahman, M. A., Mizutani, N., Kawasaki, K., 2006. Numerical modeling of dynamic responses and mooring forces of submerged floating breakwater. Coast. Eng. 53, 799-815.

Sun, B., Li, C., Yang, S., Zhang, H., Song, Z., 2022. Experimental and numerical study on the wave attenuation performance and dynamic response of kelp-box type floating breakwater. Ocean. Eng. 263, 112374.

Tang, H., Huang, C., Chen, W., 2011. Dynamics of dual pontoon floating structure for cage aquaculture in a two-dimensional numerical wave tank. J Fluid Struct. 27, 918-936.

Uzaki, K., Ikehata, Y., Matsunaga, N., 2011. Performance of the Wave Energy Dissipation of a Floating Breakwater with Truss Structures and the Quantification of Transmission Coefficients. J Coastal Res. 27, 687-697.

Wang, T., Hao, J., Wu, X., Li, Y., Wang, X., 2021. Effect of Failure Mode of Taut Mooring System on the Dynamic Response of A Semi-Submersible Platform. China Ocean Eng. 35, 841-851.

Yang, Z., Ji, X., Xie, M., Li, J., Zhang, H., Wang, D., 2021. Experimental study on the dynamic response of a water ballast type floating breakwater. Ocean. Eng. 233, 109012.

Yang, Z., Xie, M., Gao, Z., Xu, T., Guo, W., Ji, X., et al., 2018. Experimental investigation on hydrodynamic effectiveness of a water ballast type floating breakwater. Ocean. Eng. 167, 77-94.

Yin, Z., Ni, Z., Luan, Y., Zhang, X., Li, J., Li, Y., 2023. Hydrodynamic characteristics of a box-type floating breakwater with restrained piles under regular waves. Ocean. Eng. 280, 114408.

Zhang, H., Sun, B., Li, Z., Wang, F., 2023. Wave attenuation and motion response of floating breakwater with sponge material. Ocean. Eng. 277, 114325.

Zheng, Y. N., Liu, X. M., Chen, C., P, Jiang, Y. P., Zhang, C. W., 2018. Experimental study on the wave dissipation performance and mooring force of porous floating breakwater. IOP Conference Series: Earth and Environmental Science. 189, 022058.